Aus dem Institut/der Klinik für Neurochirurgie
der Medizinischen Fakultät Charité – Universitätsmedizin Berlin

DISSERTATION

In Vivo Analyse der Mikrogliadynamik im malignen Gliom

zur Erlangung des akademischen Grades
Doctor medicinae (Dr. med.)

vorgelegt der Medizinischen Fakultät
Charité – Universitätsmedizin Berlin

von

Simon Heinrich Bayerl

aus Berlin

Datum der Promotion: 10.03.2017

2. Abstrakt in Deutsch

Time Lapse *in-vivo*-Mikroskopie als Nachweis der individuellen Dynamik der Mikroglia-Tumormilieu-Interaktion – eine neue Rolle des perivaskulären Raums als Schnellstrasse für aktivierte Mikrogliazellen

Mikrogliazellen sind entscheidend für das Wachstum und den Progress von malignen Gliomen. Jedoch ist nur sehr wenig über das intratumorale Verhalten von Mikrogliazellen und die dynamische Interaktion mit dem Tumor bekannt. Aktuell basiert das begrenzte Wissen über das Erscheinungsbild der Mikroglia in Gliomen auf histologischen und in-vitro-Studien. Um das Muster der Mikrogliaaktivität und -motilität sowie die Migration der Zellen zu verstehen, haben wir eine intravitale Studie in einem orthotopen, murinen Gliommodell mit CX3CR1-eGFP$^{GFP/wt}$-Mäusen konzipiert. Wir haben die Dynamik der intratumoralen Mikroglia-Akkumulation und -aktivität und auch die Interaktion der Mikrogliazellen mit Blutgefäßen des Tumors mit intravitaler Epi- und Zwei-Photonen-Fluoreszenzmikroskopie untersucht. Zudem haben wir die zellulären Funktionen und Gewebsfunktionen einschließlich der Messung der Enzymaktivität der NADPH-Oxidase durch in-vivo-Fluoreszenz-lebenszeitmessung im Tumor und in der Mikroglia dargestellt. Zudem haben wir den Einfluss der antivaskulären Therapie auf das Verhalten der Mikrogliazellen sowie deren Migration und Proliferation untersucht.

Wir konnten drei morphologische Phänotypen von Tumor-assoziierter Mikroglia mit vollkommen unterschiedlichen Zellgrößen und Bewegungsmustern identifizieren. Im Gegensatz zu vorrausgegangenen Studien konnten wir beobachten, dass sich eine Fraktionen der Mikrogliazellen sehr schnell im Tumorgewebe bewegt und große Strecken binnen weniger Minuten zurücklegt wohingegen sich die anderen Fraktionen wenig oder gar nicht bewegen. Wir stellten fest, dass sich die NADPH-Oxidase-Aktivität in den unterschiedlichen Mikroglia-Subtypen dramatisch unterscheidet und hierdurch verschieden große Mengen von reaktiven Sauerstoffradikalen produziert werden. Dies weist auf die vielseitige Funktion der verschiedenen Mikroglia-Subtypen hin. Wir haben beobachtet, dass die größte Motilität der Mikroglia in der peri-vaskulären Nische zu finden ist, was auf die hohe Relevanz der Mikroglia-Tumorgefäß-interaktion hindeutet. Entsprechend zeigte sich unter Antivaskulärer Therapie eine relevante Gefäßreduktion im Tumor und

konsekutiv eine Abnahme der Mikrogliazellen im Gliom. Die vorgestellten Daten bestätigen die Relevanz des Tumorgefäß-Kompartiments auf die Migration und die Biologie der Mikroglia.
Zusammengefasst konnten wir neue Einsichten in das Verhalten der Mikrogliazellen *in vivo* hinsichtlich ihrer Motilität und Funktion im malignen Gliom eröffnen.

3. Abstrakt in Englisch

Time Lapse In Vivo Microscopy Reveals Distinct Dynamics of Microglia-Tumor Environment Interactions – A New Role for the Tumor Perivascular Space as Highway for Trafficking Microglia

Microglial cells are critical for glioma growth and progression. However, only little is known about intratumoral microglial behavior and the dynamic interaction with the tumor. Currently the scarce understanding of microglial appearance in malignant gliomas merely originates from histological studies and in vitro investigations. In order to understand the pattern of microglia activity, motility and migration we designed an intravital study in an orthotopic murine glioma model using CX3CR1-eGFP$^{GFP/wt}$ mice. We analysed the dynamics of intratumoral microglia accumulation and activity, as well as microglia/tumor blood vessel interaction by epi-illumination and 2-photon laser scanning microscopy. We further investigated cellular and tissue function, including the enzyme activity of intratumoral and microglial NADPH oxidase measured by *in vivo* fluorescence lifetime imaging. Furthermore we investigated the influence of antivascular therapy on microglia cell behavior, migration and proliferation within malignant gliomas.
We identified three morphological phenotypes of tumor-associated microglia cells with entirely different cell size and motility patterns. In contrast to previous studies we could observe that one fraction of microglia cells showed a very fast cell movement within the tumor tissue and covers long distances within a few minutes. We found that NADPH oxidase activation is highly divergent in these different microglia subtypes leading to distinct production levels of reactive oxygen species (ROS) indicating various functions of microglia subtypes. We observed that microglia motility

is highest within the perivascular niche, suggesting relevance of microglia/tumor blood vessel interactions. In line, a reduction of tumor blood vessels by antivascular therapy resulted in a decrease of microglia cells in gliomas. This confirmed the relevance of the tumor vessel compartment on microglia migration and its biology in brain tumors.
In summary, we provide new insights into *in vivo* microglial behavior, regarding both morphology and function, in malignant gliomas.

4.1 Eidesstattliche Versicherung

„Ich, Simon Heinrich Bayerl, versichere an Eides statt durch meine eigenhändige Unterschrift, dass ich die vorgelegte Dissertation mit dem Thema „In Vivo Analyse der Mikrogliadynamik im malignen Gliom“ selbstständig und ohne nicht offengelegte Hilfe Dritter verfasst und keine anderen als die angegebenen Quellen und Hilfsmittel genutzt habe.
Alle Stellen, die wörtlich oder dem Sinne nach auf Publikationen oder Vorträgen anderer Autoren beruhen, sind als solche in korrekter Zitierung (siehe „Uniform Requirements for Manuscripts (URM)“ des ICMJE -*www.**icmje**.org*) kenntlich gemacht. Die Abschnitte zu Methodik (insbesondere praktische Arbeiten, Laborbestimmungen, statistische Aufarbeitung) und Resultaten (insbesondere Abbildungen, Graphiken und Tabellen) entsprechen den URM (s.o) und werden von mir verantwortet.
Mein Anteil an der ausgewählten Publikation entspricht dem, der in der untenstehenden gemeinsamen Erklärung mit dem Betreuer, angegeben ist.

Die Bedeutung dieser eidesstattlichen Versicherung und die strafrechtlichen Folgen einer unwahren eidesstattlichen Versicherung (§156,161 des Strafgesetzbuches) sind mir bekannt und bewusst.“

_____
Datum/Unterschrift

4.2 Ausführliche Anteilserklärung an der erfolgten Publikation

Publikation:

Simon Heinrich Bayerl, Raluca Niesner, Zoltan Cseresnyes, Helena Radbruch, Julian Pohlan, Susan Brandenburg, Marcus Alexander Czabanka, Peter Vajkoczy, Time Lapse In Vivo Microscopy Reveals Distinct Dynamics of Microglia-Tumor Environment Interactions – A New Role for the Tumor Perivascular Space as Highway for Trafficking Microglia, *Glia*, 2016

Beitrag im Einzelnen:

Die Idee des Projekts entstammt der Arbeitsgruppe „Vascular imaging“, geleitet durch Prof. Dr. Peter Vajkoczy. Zur Untersuchung der Zell-Zell-Interaktionen habe ich die intravitale Zwei-Photonen Fluoreszenzmikroskopie für unser Model etabliert und hierfür habe ich begonnen mit der JIMI-Arbeitsgruppe zu arbeiten. Ich habe in Zusammenarbeit mit der JIMI-Arbeitsgruppe (Raluca Niesner und Zoltan Cseresnyes) die Analyseparameter zur Beschreibung der unterschiedlichen Zelltypen teilweise entworfen oder ausgewählt, nachdem ich feststellte welch große Unterschiede unter den Mikrogliazellen hinsichtlich der Morphologie und der Dynamik bestehen.
Bei der Durchführung der Versuche habe ich folgende Versuchsschritte selbständig durchgeführt:

1. In dem Projekt habe ich alle mikrochirurgischen Eingriffe zur Schädelfensterpräparationen mit und ohne Tumorimplantationen sowie alle stereotaktischen Tumorimplantationen vorgenommen.
2. Auch die Epi-Fluoreszenzmikroskopie sowie die Zwei-Photonen-Mikroskopie zu den unterschiedlichen Zeitpunkten habe ich vorgenommen.
3. Die Videoanalyse mittels unterschiedlicher Auswertungsprogrammen (CAPIMAGE, Volocity, Imaris) sind ebenfalls durch mich erfolgt.
4. Desweiteren habe ich die MRT-Diagnostik am Tier-MRT und auch die

anschließende Volumetrie mittels Analyze Direct durchgeführt.

5. Die Schockgefrierung und das Schneiden der Gefrierschnitte sowie die Färbung mit unterschiedlichen Antikörpern und Fluoreszenzfarbstoffen, die Visualisierung am Fluoreszenzmikroskop habe ich durchgeführt; auch die Auswertung der histologischen Ergebnisse ist durch mich erfolgt.
6. Das Manuskript habe ich mit Unterstützung geschrieben und auch das Figure-Design sowie die Videoformatierungen habe ich vorgenommen.

Teile des Projekts konnte ich auf verschiedenen Kongressen sowohl einem biologischen (7th International Symposium on the Biology of Endothelial Cells, Wien 2009), einem neurochirurgischen (Jahrestagung der Deutschen Gesellschaft für Neurochirurgie, Düsseldorf 2013) als auch einem neuroonkologischen (Young Investigator Meeting- Neuroonkologie, Gut Liebenberg, 2015) Kreis von Wissenschaftlern vorstellen.

_____

Unterschrift, Datum und Stempel des betreuenden Hochschullehrers

_____

Unterschrift des Doktoranden

5. Auszug aus der Journal Summary List

ISI Web of Knowledge℠

Journal Citation Reports®

WELCOME | HELP

2014 JCR Science Edition

Journal Summary List

Journal Title Changes

Journals from: subject categories NEUROSCIENCES | VIEW CATEGORY SUMMARY LIST

Sorted by: Impact Factor | SORT AGAIN

Journals 21 - 40 (of 252)

[1 | 2 | 3 | 4 | 5 | 6 | 7 | 8 | 9 | 10]

Page 2 of 13

MARK ALL | UPDATE MARKED LIST

Ranking is based on your journal and sort selections.

Mark	Rank	Abbreviated Journal Title (linked to journal information)	ISSN	JCR Data						*Eigenfactor*® Metrics	
				Total Cites	Impact Factor	5-Year Impact Factor	Immediacy Index	Articles	Cited Half-life	*Eigenfactor*® Score	*Article Influence*® Score
☐	21	NEUROSCIENTIST	1073-8584	3821	6.837	6.675	1.708	48	7.1	0.00882	2.404
☐	22	CURR OPIN NEUROBIOL	0959-4388	12732	6.628	7.284	1.604	164	8.2	0.03380	3.559
☐	23	MOL NEURODEGENER	1750-1326	2058	6.563	5.709	0.672	58	3.7	0.00873	1.797
☐	24	NEUROIMAGE	1053-8119	78028	6.357	7.289	1.500	1033	6.5	0.17239	2.257
☐	25	J NEUROSCI	0270-6474	173265	6.344	7.348	1.188	1486	8.0	0.38326	2.862
☐	26	GLIA	0894-1491	11659	6.031	5.511	1.980	147	7.4	0.02283	1.782
☐	27	HUM BRAIN MAPP	1065-9471	16505	5.969	6.687	1.176	454	6.0	0.04232	2.288
☐	28	BRAIN BEHAV IMMUN	0889-1591	8218	5.889	5.895	1.278	205	4.7	0.02239	1.728
☐	29	J PSYCHIATR NEUROSCI	1180-4882	2491	5.861	6.789	0.902	41	6.0	0.00622	2.175
☐	30	BRAIN STRUCT FUNCT	1863-2653	2478	5.618	6.935	1.354	147	3.8	0.01071	2.435
☐	31	MOL AUTISM	2040-2392	577	5.413	5.821	0.442	52	2.4	0.00308	2.045
☐	32	J NEUROINFLAMM	1742-2094	5318	5.408	5.632	0.605	215	3.2	0.01820	1.524
☐	33	J CEREBR BLOOD F MET	0271-678X	15903	5.407	5.455	0.974	232	8.0	0.02926	1.785
☐	34	CURR OPIN NEUROL	1350-7540	4789	5.307	5.004	0.828	87	6.0	0.01265	1.732
☐	35	PAIN	0304-3959	31705	5.213	6.241	1.239	284	9.6	0.05060	2.160
☐	36	MOL NEUROBIOL	0893-7648	4012	5.137	5.460	1.209	206	4.0	0.01026	1.509
☐	37	CORTEX	0010-9452	6768	5.128	5.014	0.966	178	5.8	0.01690	1.623
☐	38	NEUROPHARMACOLOGY	0028-3908	16524	5.106	4.823	1.182	417	6.0	0.03722	1.454
☐	39	NEUROBIOL DIS	0969-9961	12714	5.078	5.298	1.142	275	5.4	0.03304	1.662
☐	40	NEUROTHERAPEUTICS	1933-7213	2584	5.054	5.821	1.319	72	4.5	0.00909	1.829

Time Lapse *In Vivo* Microscopy Reveals Distinct Dynamics of Microglia-Tumor Environment Interactions—A New Role for the Tumor Perivascular Space as Highway for Trafficking Microglia

Simon Heinrich Bayerl,[1] Raluca Niesner,[2] Zoltan Cseresnyes,[2] Helena Radbruch,[3] Julian Pohlan,[2] Susan Brandenburg,[1] Marcus Alexander Czabanka,[1] and Peter Vajkoczy[1]

Microglial cells are critical for glioma growth and progression. However, only little is known about intratumoral microglial behavior and the dynamic interaction with the tumor. Currently the scarce understanding of microglial appearance in malignant gliomas merely originates from histological studies and *in vitro* investigations. In order to understand the pattern of microglia activity, motility and migration we designed an intravital study in an orthotopic murine glioma model using CX3CR1-eGFP$^{GFP/wt}$ mice. We analysed the dynamics of intratumoral microglia accumulation and activity, as well as microglia/tumor blood vessel interaction by epi-illumination and 2-photon laser scanning microscopy. We further investigated cellular and tissue function, including the enzyme activity of intratumoral and microglial NADPH oxidase measured by *in vivo* fluorescence lifetime imaging. We identified three morphological phenotypes of tumor-associated microglia cells with entirely different motility patterns. We found that NADPH oxidase activation is highly divergent in these microglia subtypes leading to different production levels of reactive oxygen species (ROS). We observed that microglia motility is highest within the perivascular niche, suggesting relevance of microglia/tumor blood vessel interactions. In line, reduction of tumor blood vessels by antivascular therapy confirmed the relevance of the tumor vessel compartment on microglia biology in brain tumors. In summary, we provide new insights into *in vivo* microglial behavior, regarding both morphology and function, in malignant gliomas.

GLIA 2016;64:1210–1226

Key words: glioma, microglia motility, 2 photon microscopy, NADPH oxidase, angiogenesis

Introduction

Microglia plays an important role in the development and prognosis of malignant gliomas (Morimura et al., 1990; Roggendorf et al., 1996). It contributes significantly to the tumor mass (5-30%). Gliomas with a high number of microglial cells are associated with a distinct edema (Shinonaga et al., 1988). Microglial cells seem to migrate into the tumor area even from the contralateral hemisphere (Morioka et al., 1992). Glioma cells induce microglial migration via diverse chemokines (Kielian et al., 2002; Wang et al., 2012). The role of microglial cells in malignant glioma is still heavily disputed. For instance, several studies suggest, that microglia cells contribute to tumor proliferation and infiltration because the microglial defense function is compromised in the tumor area (Coniglio et al., 2012; Flügel et al., 1999; Markovic et al., 2009; Sahm et al., 2013; Zhai et al., 2011). On the other hand, anti-tumor effects of microglial cells could be detected as well (Galarneau et al., 2007; Wei et al., 2013). Consequently the current literature seems to suggest that its predominant role is rather tumor supporting than tumor

View this article online at wileyonlinelibrary.com. DOI: 10.1002/glia.22994

Published online May 3, 2016 in Wiley Online Library (wileyonlinelibrary.com). Received Mar 8, 2016, Accepted for publication Apr 8, 2016.

Address correspondence to Peter Vajkoczy, MD, Department of Neurosurgery, Charité Universitätsmedizin Berlin, Augustenburger Platz 1, Berlin 13353, Germany. E-mail: peter.vajkoczy@charite.de

From the [1]Department of Neurosurgery, Charité Universitätsmedizin Berlin, Augustenburger Platz 1, Berlin, Germany; [2]German Rheumatism Research Center Berlin, Berlin, Germany, Charitéplatz 1, Berlin, Germany; [3]Department of Neuropathology, Charité Universitätsmedizin Berlin, Charitéplatz 1, Berlin, Germany.

Additional Supporting Information may be found in the online version of this article.

suppressing. Thus, the modulation of microglia appears to be a promising anti-tumor therapy (Hussain et al., 2007; Pyonteck et al., 2013; Sarkar et al., 2013; Zemp et al., 2014).

Microglial cells may appear in various morphological and immunological phenotypes. In the current literature, two morphological microglia phenotypes have been described: First, resting microglia with ramified branches, which survey and communicate with the microenvironment, and second, activated amoeboid type microglia with short and thick processes, which synthesize cytokines, chemokines and reactive oxygen species (ROS), that also interact under pathological conditions (Graeber et al., 2002; Kloss et al., 2001). Several studies demonstrated the activation of microglia cells, as well as their differentiation from the resting to the activated phenotype in neurodegenerative, inflammatory, trauma and tumor diseases. Since these reports are based on histoanalytical techniques, our understanding of microglia cell motility and dynamics is scarce. Intravital analysis of microglial dynamics in rodent CNS-disease models have illustrated changes of process dynamics, which also occur in elderly rodent brains. Only very small movements of cell bodies could be detected in trauma and degeneration (1–2 μm/h) (Davalos et al., 2005; Hefendehl et al., 2014; Hines et al., 2009; Kozlowski and Weimer, 2012; Nimmerjahn et al., 2005; Tremblay et al., 2010; Wake et al., 2009). In contrast, the kinetics and dynamics of microglial cell trafficking in malignant glioma have not yet been examined.

Thus, we set out to investigate the dynamics of microglia activation, change in microglia morphology and microglia trafficking kinetics, as well as their enzyme activities in malignant gliomas using *in vivo* time-lapse microscopic techniques. In addition, we also focused on the interplay of microglial cells with tumor blood vessels and its dependence on tumor angiogenesis. To this end, we combined *in vivo* epifluorescence video microscopy and *in vivo* Two-photon laser scanning microscopy (TPLSM) in order to image a murine orthotopic glioma via a transparent chamber model. This allowed us to provide unique insights into the *in vivo* behavior of microglial cells within the glioma microenvironment.

Abbreviations

CCD	Charge-coupled device
FLIM	Fluorescence lifetime imaging
IEFVM	Intravital epi-illuminating Fluorescence video microscopy
MRI	Magnet Resonance Imaging
NADPH	Nicotinamide adenine dinucleotide phosphate
PBS	Phosphate buffered saline
PDGFR	Platelet-derived growths factor receptor
ROS	Reactive oxygen species
TPLSM	Two-Photon Laser Scanning Microscopy
TVD	Total vascular density
VEGF	Vascular endothelial growth factor

Materials and Methods

Animals

Mice were kept and bred at the local animal facility. CX3CR1$^{GFP/wt}$ mice (B6.129P-Cx3cr1tm1Litt/J, Jackson Laboratory, Bar Habour, USA) were used to identify microglia cells. All animal experiments were approved by the local government authorities (Landesamt für Gesundheit und Soziales (LaGeSo); G0152/09).

Tumor Cells

As the GL261-glioma model was shown to deliver a realistic immunocompetent, orthotopic murine tumor growth with glioma like angiogenesis and necrosis, we decided to use this model for our experiments (Oh et al., 2014). GL261 cells were cultured in DMEM (Dulbecco's Modified Eagle's Medium) with 4.5 g/l glucose and pyruvate supplemented, 10% fetal bovine Serum, 100 U/ml penicillin and 100 μg/ml streptomycin at 37°C in 5% CO_2 humidified incubators.

Surgeries and Antivascular Therapy

As an orthotopic glioma model murine Gl261 cells were implanted into CX3CR1$^{GFP/wt}$ mice. Before the surgical procedure mice were anesthetized with intraperitoneal injection of ketamine (90 mg/kg) and xylazine (10 mg/kg).

Chronic cranial window preparation. For intravital microscopy a fronto-parietal chronic cranial window preparation was performed and the dural layer was removed according to previous publications (Yuan et al., 1994). 1x10^5 GL261 cells were implanted. For epifluorescence microscopy, cells were placed epi-pial onto the brain surface. For intravital TPLSM, cells were stereotactically injected into the brain parenchyma using a 1 μl Hamilton microsyringe. Cells were injected 1 mm lateral to the sagittal sinus into a depth of 500 μm (Winkler et al., 2009). Baseline groups with physiological conditions received surgery without tumor cell implantation.

Stereotactic tumor cell implantation. For MRI imaging and histological analysis 5×10^4 GL 261 cells were implanted stereotactically into CX3CR1 $^{GFP/wt}$ mice. Injection was performed in a stereotactic head holder 1mm frontal and 2 mm lateral to the bregma to a depth of 3 mm. Baseline groups received stereotactic procedure without cell implantation.

Antivascular therapy. Animals in treatment groups received daily intraperitoneal antivascular Sunitinib therapy starting on day 10 after tumor cell implantation until the end of the experiment (40 mg/kg body weight, SU11248). Control groups received intraperitoneal phosphate buffered saline (PBS) injections.

Immune Fluorescence Staining

21 days after tumor cell implantation, the animals were perfused with 4% paraformaldehyde solution and decapitated. Fresh frozen brain slices of 4 μm thickness were generated. Brain sections were thawed and incubated with blocking buffer (1× PBS containing 0.5% Casein, Sigma Aldrich) for 30 minutes. Primary antibody staining with monoclonal rabbit anti-CD31 antibody, rat anti-KI67 antibody and goat anti-Iba-1 antibody (Abcam, 1:100) in PBS/0.5%

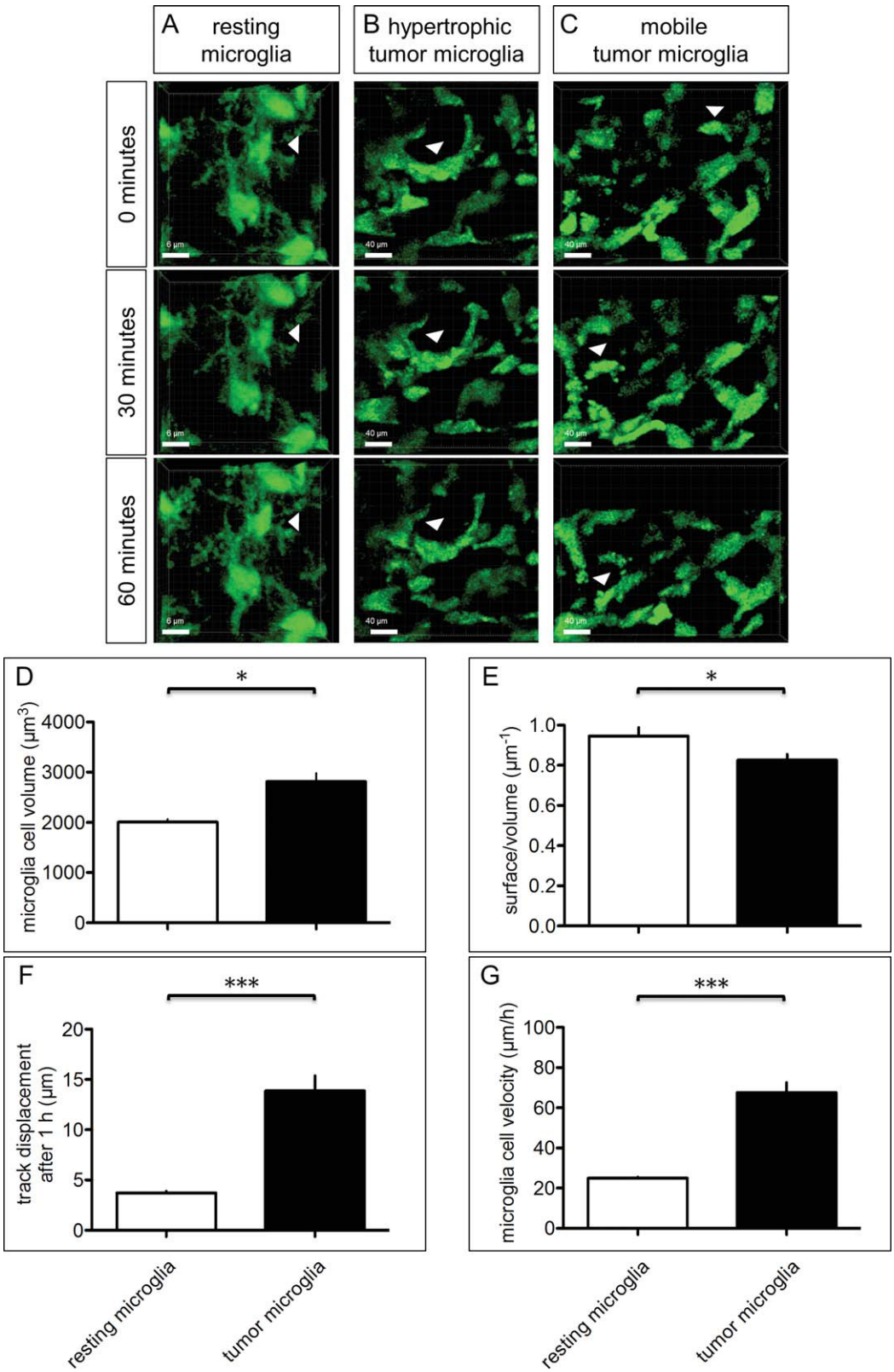

FIGURE 1: Microglia velocity, shape and size in GL261-glioma and physiological cortex measured by intravital TPLSM on day 14 after tumor cell implantation. Upper part: representative screenshots of movies to analyze motion, shape and size of microglia cells in physiological conditions and in gliomas: (A) resting microglia in physiological condition with ramified processes, not significantly moving in 30/60 minutes. (B) hypertrophic, stationary tumor microglia cell, which are not significantly moving in 30/60 minutes (C) small tumor microglia, which moves quickly in 30/60 minutes. Lower part: Quantification of microglia size, shape and velocity: (D) cell volume of tumor microglia is significantly higher compared to resting microglia. (E) surface/ volume ratio is significantly smaller in tumor microglia, due to greater cell size, round cell bodies and reduced cell processes. (F) mean track displacement/ time (distance between the cell location at time point 0 and in the end of the movie per time) is increased in tumor microglia because of a significant cell movement in a fraction of tumor associated microglia cells. (G) mean cell velocity is higher in tumor microglia because of a high cell motility in a fraction of tumor associated microglia cells. *P <0.05, ***P <0.001.

Casein was added. Two hours later the sections were washed with the blocking solution and treated with the secondary antibody for 1.5 hours (JacksonImmunoResearch Laboratory, 1:200). Slides were washed again and covered with DAPI-containing mounting medium (Dianova). Imaging was performed using twentyfold magnification with a Zeiss Axio Observer Z1 fluorescence microscope (Zeiss

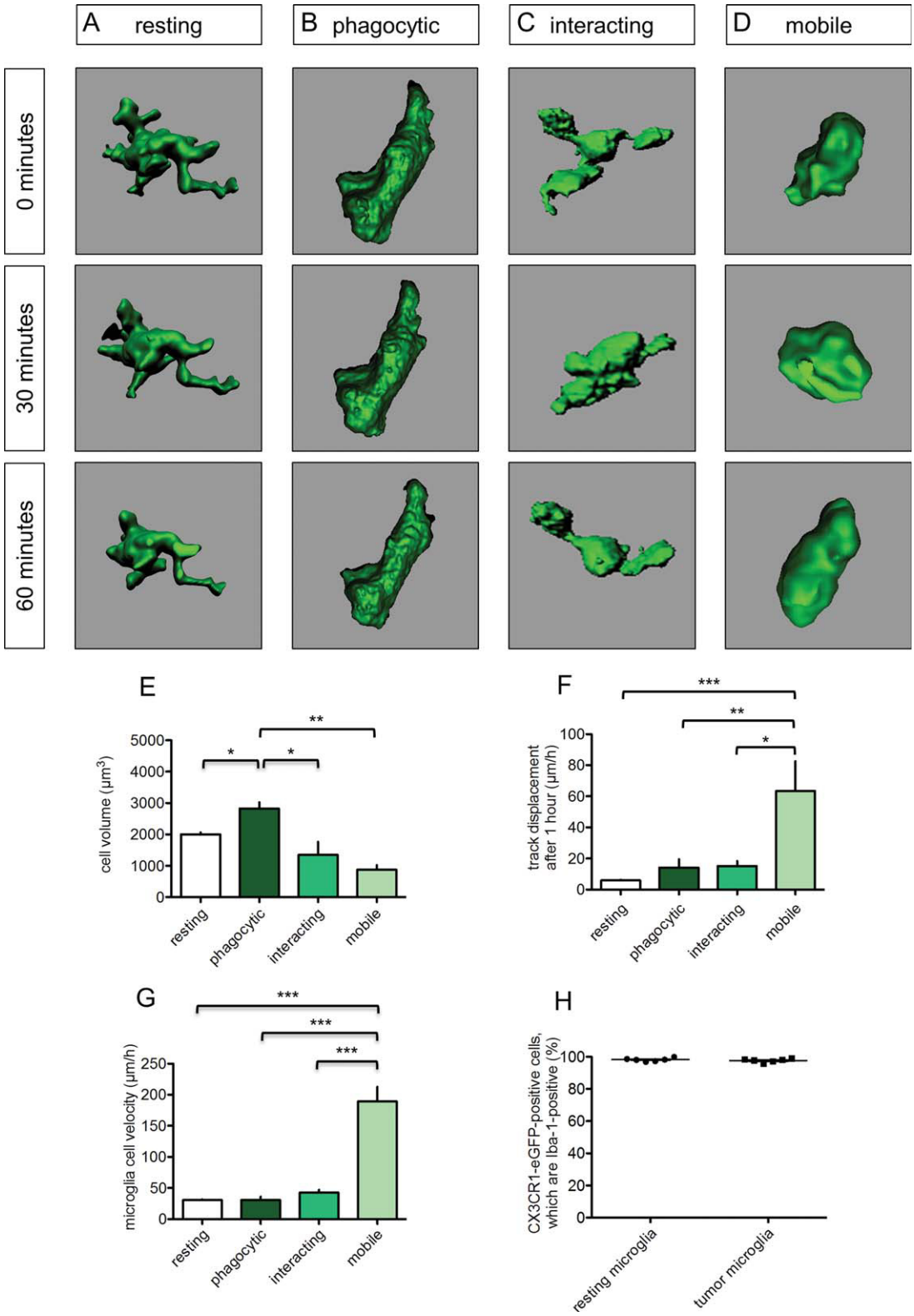

FIGURE 2.

MicroImaging GmbH, Jena, Germany). For quantification of vascularization the vessel area (area of all vessels/mm^2) and the vessel density (number of vessels/mm^2) was determined. Microglial accumulation was measured by counting microglia cells per area (n/mm^2). The percentage of perivascular microglia was ascertained, defined as the ratio of microglia cells with direct contact to endothelial cells. Proliferation was determined by the number of KI-67 positive microglial cells. Separately we measured the number of perivascular KI-67 positive microglia. To control the labeling of microglia cells with GFP, we counted GFP- and Iba-1 positive cells and calculated the percentage of double-positive cells.

Intravital Magnet Resonance Imaging (MRI) and Quantification

Imaging. In order to quantify tumor growth and edema in dependency of tumor angiogenesis we performed MRI imaging 21 days after stereotactic tumor cell implantation. For the duration of scanning animals received isofluran anesthesia. We investigated 2 groups: 1. Control group ($n = 8$) with tumor cell implantation and no treatment 2. Treatment group ($n = 8$) with tumor cell implantation and antivascular therapy starting on day 10 after cell implantation. Measurements were completed on day 21 of the tumor growth. Magnetic resonance imaging was performed with a 7T scanner (Pharmascan 70/16 AS, Bruker BioSpin MRI GmbH, Ettlingen Germany) with actively shielded gradient coils (300 mT/m, rise time 80 μs). The radio frequency transmission and reception were achieved with a 20 mm (inner diameter) quadrature mouse head volume resonator (RAPID Biomedical, Würzburg, Germany). Body temperature was maintained with a heated circulation water blanked whilst being continuously monitored together with the respiration rate (Small Animal Instruments, Stony Brook, NY). The imaging protocol was completed within 20 minutes. It consisted of a T1- and T2-weighted spin-echo sequence (T2 sequence: TR/TE = 4200/36ms, Rare factor 8, 4 averages; post-contrast T1: TR/TE = 800/10.6ms, Rare factor 2, 4 average). We performed 20 axial slices with a slice thickness of 0,5 mm. A field of view 2.56 × 2.56 cm and a matrix of 256 × 256 was positioned between the olfactory bulb and cerebellum.

Image analysis. Volumetric analysis of the tumor area and the edema was performed using Analyze Imaging Software 7.5 (Analyze Direct, Inc.; Lenexa USA). Hyperintense areas in T2-weighted images as well as contrast enhancing areas in T1-weighted images were marked with a region of interest tool. Pixel-based image segmentation results in a 3D object map of the whole tumor region. Tumor volume was automatically calculated from contrast enhancing images in T1 sequences. Bright T2-hyperintense area around the tumor mass (Hypointense area or contrast enhancing area in T1 weighted imaging) was considered as peritumoral edema (Mabray et al., 2015; Pope et al., 2005). The edema area might be accompanied by a diffuse glioma cell infiltration in these areas.

Intravital Epi-Illuminating Fluorescence Video Microscopy (IEFVM)

For the analysis of vascular parameters, hemodynamic parameters and changes during angiogenesis we performed intravital epi-illuminating fluorescence video microscopy. Three groups were analyzed: 1. Baseline group ($n = 6$) without tumor. 2. Control group ($n = 8$) with tumor cell implantation but without treatment ($n = 8$) and 3. Treatment group ($n = 8$) with tumor cell implantation and antivascular therapy starting on day 10. Intraperitoneal ketamine- and xylazine-anesthesia was implemented and animals were fixed in a head holder. To visualize microvessels, 2% FITC conjugated dextran (Fluorescein Isothiocyanate, 0.1 ml, 150.000, Sigma) was applied intravenously. For measurements of monocyte and lymphocyte recruitment and to illustrate white blood cell-endothelial cell interaction, 0.2% rhodamine 6G (0.1 ml; Sigma) was injected as a fluorescent tracer for white blood cells including granulocytes, lymphocytes and monocytes (Baatz et al., 1995). Microscopy was performed on day 3, 6, 9, 12, 15, 18 and 21 after cell implantation. 4-8 areas of interest per point in time per animal were recorded with a water immersion microscope objective lens with twentyfold magnification. For IEFVM an Axiotech vario microscope was used (Attoarc; Zeiss, Jena, Germany) with a blue (450–490 nm) and green (520–570 nm) filter block. Images were recorded by a charge-coupled device (CCD) video camera with an optional image intensifier designed to detect weak fluorescence signals (Kappa, Gleichen, Germany). Afterwards images were transferred to a S-VHS video system (Panasonic) for offline analysis using a computer assisted analysis system (CAPIMAGE; Zeintl Software Engineering, Heidelberg, Germany). Of the microcirculatory parameters we determined the total vessel density (length of vessels/area (cm^{-1}), Microvascular permeability (P) was determined as the ratio between intra- and extravascular contrast illustrating FITC-dextran leakage (Vajkoczy et al., 1998).

FIGURE 2: Tumor associated microglia subtypes with differences in cell shape, cell volume, cell velocity and track displacement measured by intravital two-photon laser scanning microscopy on day 14 after tumor cell implantation. Upper part: representative screenshots of cell shape and shape changes of microglia subtypes after 30/60 minutes: (A) cell shape of not activated microglia cell in physiological brain parenchyma changes barely through moving cellular processes. (B) activated, hypertrophic phagocytic tumor microglia subtype with slight membrane motility and nearly no shape changes in 60 minutes. (C) interacting tumor microglia subtype with high motility; probing processes cause distinct shape changes during 60 minutes. (D) mobile tumor microglia subtype with amoeboid cell shape changes for fast movement through tumor tissue. Lower part: quantification of size, velocity and cell displacement of microglia subtypes: (E) cell volume quantification of microglia subtypes; phagocytic microglia subtype shows significantly greater size compared to not activated and dynamic tumor microglia subtypes. (F) quantification of cell velocity of microglia subtypes; mobile subtype shows significantly faster cell movement compared to other phenotypes. (G) quantification of track displacement (distance between the cell location at time point 0 and in the end of the movie per time) of microglia subtypes; mobile cell type shows significantly increased cell delocalization after one hour. (H) in immune fluorescence a co-staining of CX3CR1-eGFP-positive cells with Iba-1 shows about 99% of accordance in resting microglia as well as in tumor microglia. *P <0.05, **P <0.01, ***P <0.001

White blood cells, that adhered to the endothelium for at least 30 seconds were considered as sticking white blood cells. White blood cells that were moving slowly whilst in contact with the vessel wall were considered as rolling white blood cells. We measured the amount in randomly chosen 100 µm segments of venules or tumor vessels with similar size.

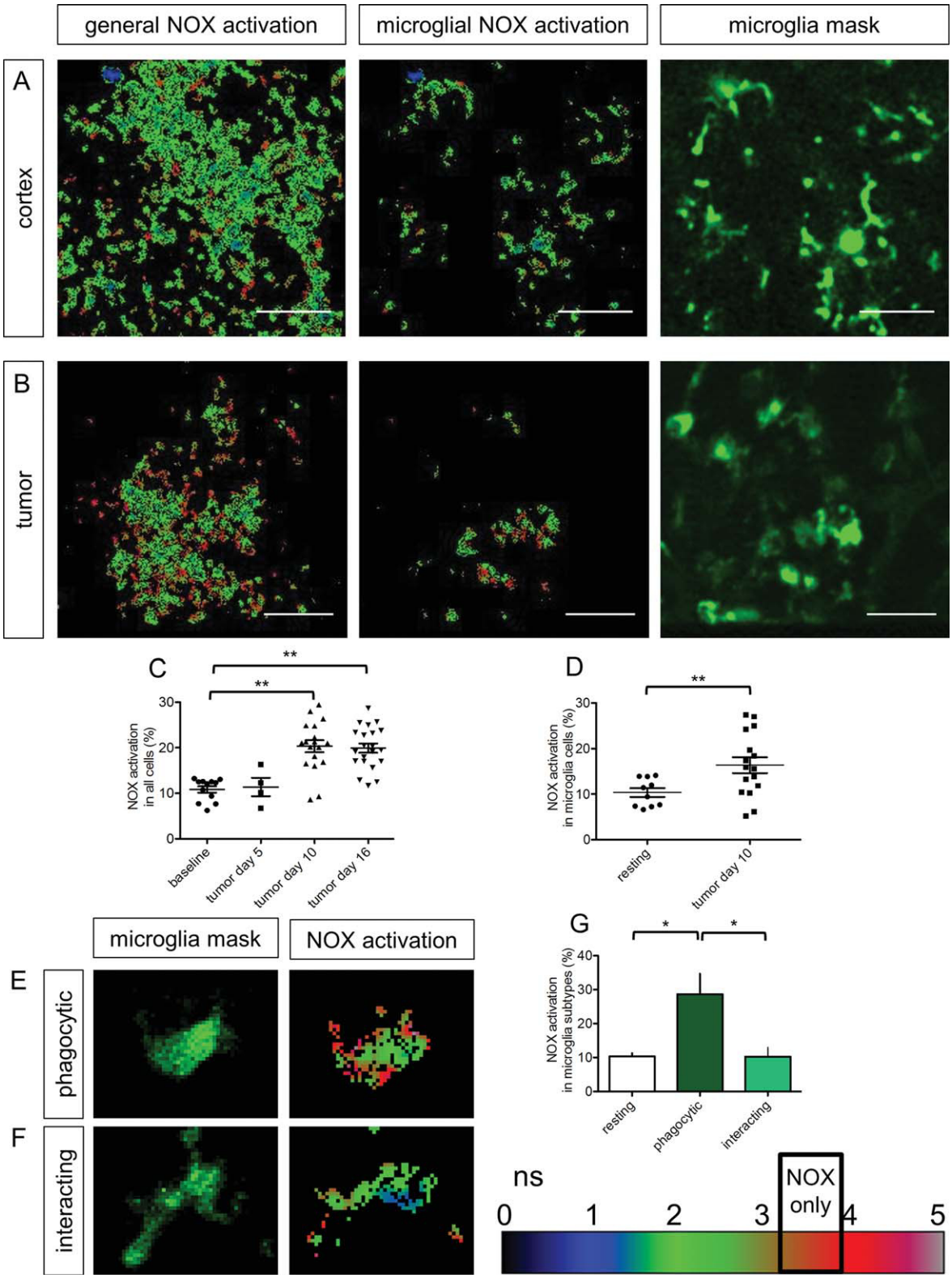

FIGURE 3.

Intravital Two-Photon Laser Scanning Microscopy (TPLSM)

Using epi-illumination microscopy, we were not able to determine microglia-vessel contact and interaction, cell dynamics and microglia migration within the tumor tissue. Specifically for the examination of intra-tumoral cell-cell interaction and cell migration, we applied an intra-axial model. Consequently we implemented intravital two-photon microscopy in order to visualize the tissue at greater depths. Cells were implanted intraparenchymally as described above. Three groups were investigated: (1) Baseline group ($n = 6$) without tumor. (2) Control group ($n = 6$) with tumor cell implantation without treatment ($n = 6$) and (3) Treatment group ($n = 6$) with tumor cell implantation and antivascular therapy starting on day 10. TPLSM was performed on day 5, 10, 12, 14, 16 and 18 after tumor cell implantation. Mice were anesthetized and positioned in a head holder. For vessel visualization 2% rhodamine B conjugated dextran (2.000.000, Sigma) was intravenously injected. Body temperature of mice was kept constant with a heating plate. Four to eight (Z) stacks and additionally a movie of 30 to 60 minutes were recorded in every animal at every point of time of development. The imaging depth was 200–800 μm below the tissue surface in the tumor area. Imaging was done using a specialized multi-photon laser-scanning microscope (LaVision Biotec GmbH, Bielefeld) with a tunable fs-pulsed Ti:Sa laser (wavelength range 700–1020 nm, 100 fs, 80 MHz, MaiTai, Spectra Physics, Germany). For imaging EGFP in the CX3CR1 mouse a wavelength of 830 nm was used. The ubiquitous endogenous coenzymes NADH and NADPH (labeled hereafter as NAD(P)H) were excited at 760 nm and detected at 460 ± 30 nm. For all experiments, an objective lens for deep-tissue imaging (20x dipping lens, NA 0.95, WD 2 mm – Olympus, Hamburg, Germany) was used.

Quantification of microglia accumulation, angiogenesis and microglia-vessel interaction. Analysis of microglia accumulation, angiogenesis and microglia vessel interaction was performed using Volocity 3D analysis software 6.3 (PerkinElmer, Waltham, Massachusetts, USA). From every z-stack, we calculated microglia volume, vessel volume and microglia-vessel co-localization surface. The amount of microglia accumulation was determined by measuring the total microglia volume and dividing it by the tumor volume (Fig. 7A). The vascularization was specified by the value of the vessel volume/tumor volume ratio (Fig. 7B). The amount of microglia-vessel co-localization was indicated by the co-localization surface/microglia volume and the co-localization surface/vessel volume ratios (Fig. 7C).

Quantification of microglia cell motility. Movies were recorded in tumor groups and the physiological group. Central tumor areas were identified in control and treatment groups. A z-stack of 300 x 300 x 50 μm was detected and one z-stack per minute was recorded for 30 to 60 minutes. The Imaris imaging software, version 7.6 X64 (Bitplane, Zurich, Switzerland) was used for 4D analysis of microglia cells. Cell volume, surface, velocity and track displacement per time were calculated. The ratio of cell surface and cell volume served as a characteristic of cell shape. The smaller the surface per volume ratio, the more round the microglia cell and the less presence of cell processes. Tumor associated microglia and physiological microglia were compared.

Characterization of microglia cells. In the tumor movies recorded from the tumor, we observed three significantly different phenotypes of tumor-associated microglia cells. All CX3CR1-positive cells could be assigned to one of these three cell types. Each cell was tracked and the cell velocity, size, track displacement per time and cell shape were compared in order to define the phenotypes quantitatively. Intratumoral quantification of microglial cell size, shape and movement were performed on day 14 after tumor cell implantation.

Fluorescence lifetime imaging (FLIM) of NADPH oxidase activity. Nicotinamide adenine dinucleotide phosphate (NADPH) oxidase (NOX) activity was measured intravitally as a parameter for production of massive ROS, and thus a marker for cells participating in oxidative stress (Niesner et al., 2008). FLIM for selective detection of NOX activity was performed in the baseline group and in the tumor groups on day 5, 10 and 16 after tumor cell implantation. First a z-stack with an excitation wavelength of 830 nm was generated in order to create a microglia and vessel mask. This was immediately followed by NAD(P)H-fluorescence lifetime imaging (FLIM) for NOX activity measurements with an excitation wavelength of 760 nm. The fluorescence decay of the coenzymes NADH and NADPH (hereafter, NAD(P)H) was approximated by a bi-exponential function, according to extensive evidence in literature (Lakowicz et al., 1992). As expected, we retrieved the short fluorescence lifetime of free NAD(P)H around 450 ps and a long fluorescence lifetime τ_2 for NAD(P)H bound to enzymes (Lakowicz et al., 1992). In contrast to NAD(P)H-dependent enzymes governing basic cellular processes, the members of the NOX family show a much longer, specific fluorescence lifetime τ_2 when bound to NAD(P)H, i.e., 3650 ps as compared to ~2000 ps (Niesner et al., 2008). Hence, acquiring the τ_2 NAD(P)H-FLIM image under intravital conditions allowed us to identify the

FIGURE 3: NADPH oxidase activity (NOX) measurements of physiological parenchyma, tumor tissue and microglia cells by fluorescence lifetime imaging. Upper part: screenshots of fluorescence lifetime measurements with NOX activity (excitation wavelength 770 nm, fluorescence lifetime (3-4 ps) in orange area of the scale at the right bottom. (A) fluorescence lifetime imaging of healthy brain parenchyma, left: fluorescence lifetime of the physiological parenchyma with low NOX activity (orange). central: fluorescence lifetime of resting microglia cells with low NOX activity (orange). right: CX3CR1-eGFP (microglia) mask corresponding to central image with NOX activation. (B) fluorescence lifetime imaging of glioma area. left: fluorescence lifetime of tumor tissue with high NOX activation (orange). central: fluorescence lifetime imaging of tumor associated microglia with high NOX activation (orange). right: CX3CR1-eGFP (microglia) mask corresponding to central image with NOX activation. Middle part: quantification of NOX activation: (C) NOX activation is increased in all cells in advanced tumor stages. (D) NOX activation is increased in tumor microglia cells compared to physiological brain parenchyma. Lower part: fluorescence lifetime imaging of microglia subtypes: (E) phagocytic tumor microglia subtype. Left, CX3CR1-eGFP (microglia) mask. Right, corresponding fluorescence lifetime with very high NOX activation (orange). (F) interacting tumor microglia subtype. left, microglia mask. right, corresponding fluorescence lifetime with low NOX activation (orange). (G) quantification of NOX activation in microglia subtypes with significantly increased NOX activation in phagocytic tumor microglia subtype compared to interacting microglia subtype and resting microglia. *$P < 0.05$, **$P < 0.01$.

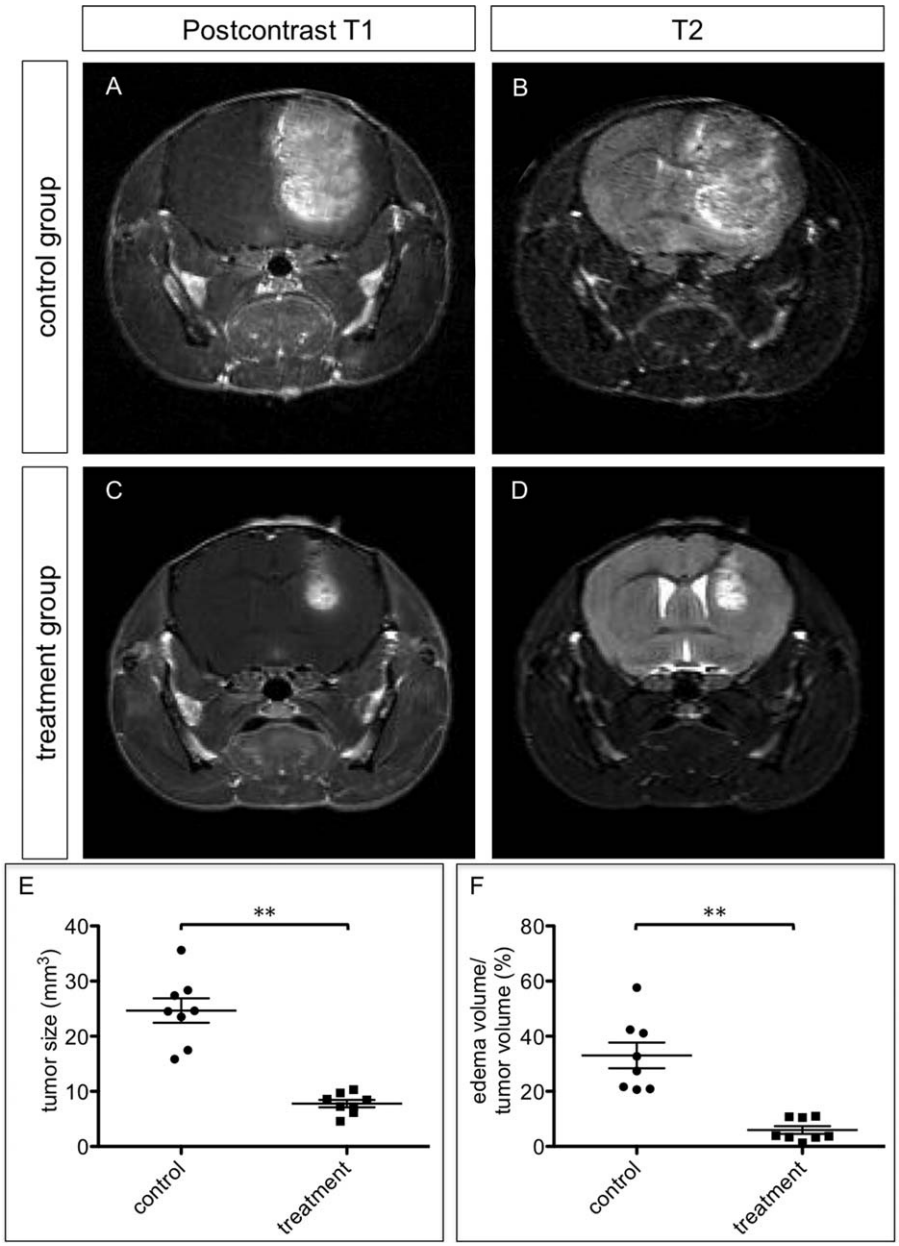

FIGURE 4: MRI measurements of gliomas in CX3CR1GFP/wt mice 21 days after GL261 cell implantation in control group and treatment group (Sunitinib treatment starting on day 10). Upper part: Representative MRI images of tumor size and edema in control and treatment group: (A) postcontrast T1-weighted and T2-weighted imaging of a representative glioma in control group shows a big tumor with distinct edema. (B) Postcontrast T1-weighted and T2-weighted imaging of a glioma, which was treated with Sunitinib, shows a small tumor size and edema. (C) Quantification of glioma size in treatment group and control group ascertained as the volume of contrast enhancing tumor in T1-weighted images. (D) Quantification of edema size in treatment group and control group calculated as the volume of contrast enhancement in T1-weigthed images substracted from the volume of hyperintensity in T2-weighted images; edema size is indicated as edema volume/ tumor volume. **$P < 0.01$.

localization of activated/functional NADPH oxidase, i.e., the source of oxidative stress *in vivo*.

Statistical Analysis

Statistical analysis was performed with GraphPad Prism 5.0c (San Diego, CA). Results with P values below 0.05 were considered as significant. Results were presented as mean and standard deviation.

Results

Morphology and Motility Substantially Change in Tumor-Activated Microglia

100 microglia cells in physiological brain parenchyma and 100 microglia cells in tumor tissue were individually tracked to examine cell size, surface, velocity and track displacement (i.e., the distance between the location of a cell at the

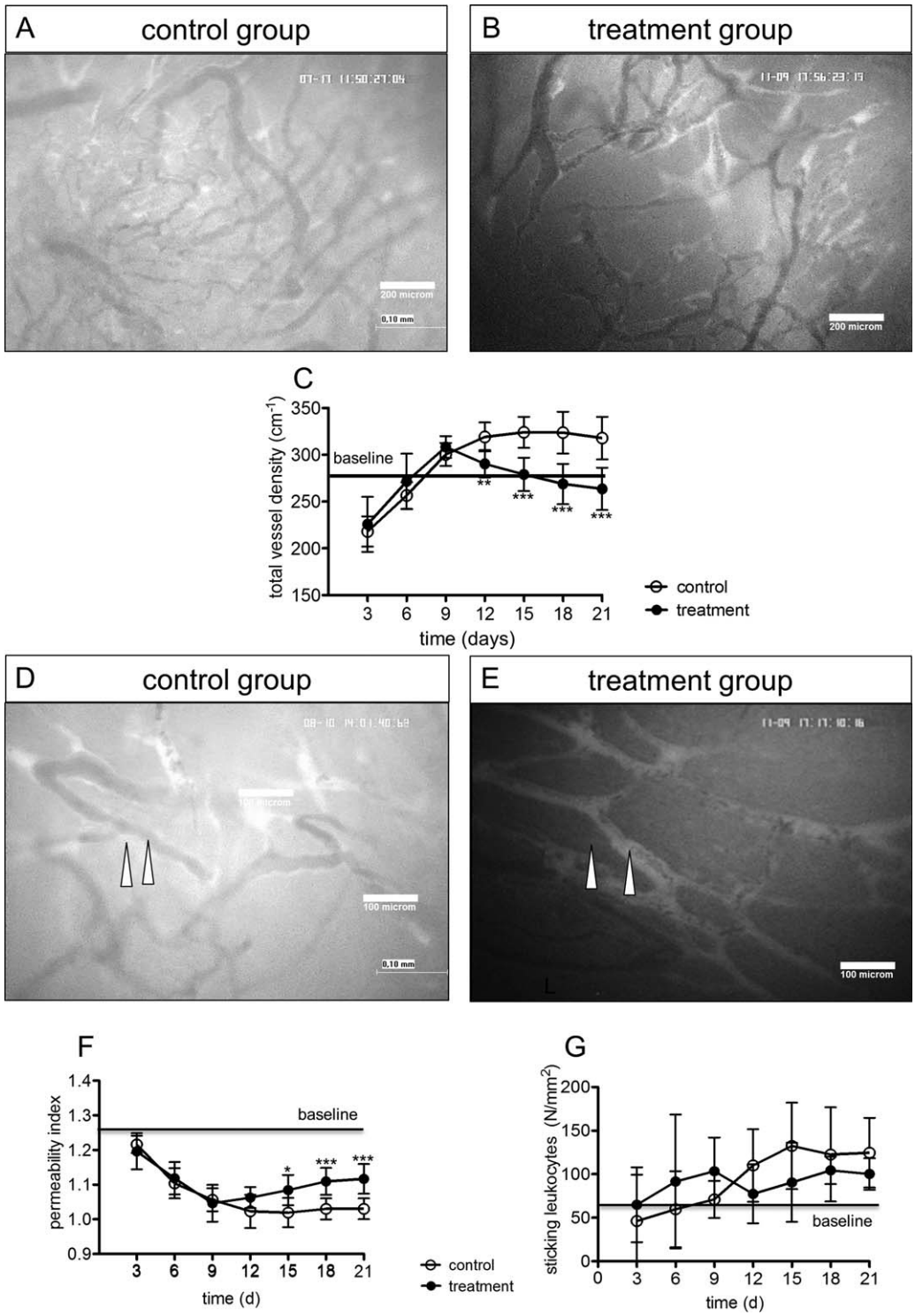

FIGURE 5: Intravital epi-illuminating fluorescence video microscopy (IEFVM) of GL261 gliomas in control group, treatment group (Sunitinib treatment starting on day 10) and baseline group (physiological group without tumor). Representative screenshots of IEFVM in control group and treatment group: (A) control group with high total vessel density. (B) treatment group with reduced total vessel density compared to control group. (C), Quantification of total vessel density, which is reduced in treatment group compared to control group from day 12 on. (D) control group with high vascular leakage of FITC-dextran resulting in a high fluorescence intensity extravascular compared to intravascular (white arrows). (E) treatment group with reduced vascular leakage of FITC-dextran resulting in a low fluorescence intensity extravascular compared to intravascular (white arrows), vessels show a high mean diameter in treatment group compared to control group. (F) Quantification of the permeability index, which decreases during tumor angiogenesis; a reduced vascular leakage with a higher permeability index can be seen in normalized vessels of treatment group (G) Quantification shows no significant increase of sticking white blood cells in tumor groups. *$P<0.05$, **$P<0.01$, ***$P<0.001$.

beginning and at the end of time series). Microglia cells in the baseline group were of small size and showed an intensive movement of the cell branches without any significant dislocation of the cell body or measurable track displacement after 1 hour (Fig. 1A, Supporting Information Movie 1). In contrast, tumor microglia appeared impressively dissimilar.

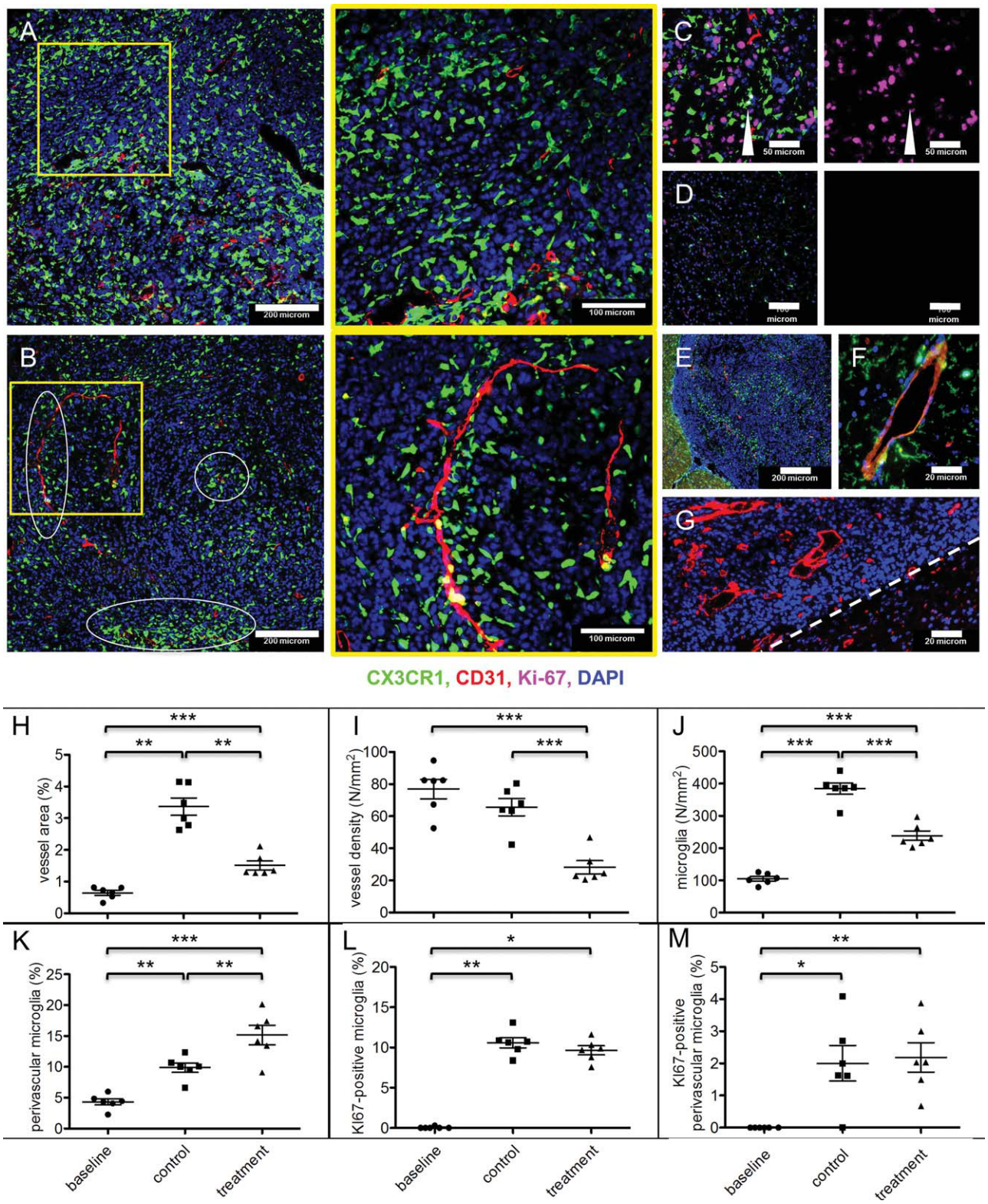

FIGURE 6.

Not only was the morphology of the cells more round with fewer processes, but many of the tumor associated microglia cells also differentiated to a highly dynamic fast moving phenotype (Fig. 1B,C Supporting Information Movie 2). All in all, intratumoral microglia cells were significantly larger with a higher cell velocity and consequently higher track displacement per time. Furthermore microglia in the tumor regions had a smaller surface-to-volume ratio indicating that cells were more round and less ramified. (Fig. 1D–G) As already investigated in the same tumor model with C57/Bl6/J mice and GL261 cells, the majority of CX3CR1-positive cells are resident microglia cells and only in the late stage of tumor growth macrophages contribute to the myeloid cell compartment. (Müller et al., 2014)

TPLSM of tumor microglia further revealed that they did not represent one uniform cell cohort but rather appeared like different tumor microglia cell types regarding size, morphology and motility. Based on distinct phenotypes and motility patterns, we classified tumor microglia into three subgroups that differed from non-activated, resting microglia in physiological brain tissue (Fig. 2A). The phenotype with the largest cell volume (phagocytic type) is characterized by a huge soma with nearly no processes (Fig. 2B,G) and without significant cell body movement, except for a slight motility of the cell membrane (Fig. 2E,F). Their general size and the presence of additional small intracellular structures with pronounced autofluorescence suggest a phagocytic function of this phenotype (Supporting Information Movie 3). The second phenotype (interacting type) shows a very motile cell membrane with fast moving thick processes (Fig. 2C). This cell type does not show a substantial range of cell body movement either (Fig. 2E,F), but is probing very actively in the immediate surrounding microenvironment (Supporting Information Movie 4). The third type (mobile type) describes a very fast moving amoeboid-like cell with almost no processes (Fig. 2D). This "mobile phenotype" is the fastest microglia phenotype and travels large distances within the tumor in a few minutes (Fig. 2E,F). It has a very small and round cell body (Supporting Information Movie 5). Interestingly, these cells have a high association to the perivascular niche and primarily migrate along the tumor vasculature (Supporting Information Movie 6).

To verify that CX3CR1-positive cells of CX3CR1$^{GFP/wt}$ mice highlight all microglia cells and are specific for microglia cells/macrophages we performed a co-staining with IBA-1 antibody in histological analysis. 99% co-staining rates of IBA-1 positive microglia cells/macrophages cells and CX3CR1-eGFP positive cells confirmed that CX3CR1-eGFP positive cells reflect the whole activated microglia/macrophage population (Fig. 2H).

NADPH-Oxidase Activity in Different Microglia Phenotypes

Different morphology and cell behavior of microglia cells imply that cells have various functions. The NADPH-oxidase enzyme activity - responsible for the production of ROS - is critical for intra- and extracellular oxidative stress and essential for phagocytosis. We measured the NADPH oxidase (NOX) activity intravitally in healthy tissue and tumor tissue by *Fluorescence live time imaging (*FLIM) to functionally distinguish between different microglia cells. In FLIM measurements of NOX activity we were able to detect the source of an increased production of ROS in tumor tissue compared to physiological tissue (Fig. 3A–C). Using EGFP fluorescence to identify the CX3CR1+ cells, we could reveal a significant increase of NOX activation in tumor microglia compared to physiological microglia (Fig. 3A,B,D). Comparing different phenotypes of tumor-associated microglia we could observe a distinct increase of NOX activation (oxidative stress) in the phagocytic phenotype (Fig. 3E,G). Again this supports the phagocytozing function of these cells. The interacting tumor microglia phenotype showed a significant lower NOX activation with the same level of ROS production as resting

FIGURE 6: Immunofluorescence staining of CX3CR1GFP/wt mice in baseline group (BG, physiological group) control group with GL261 gliomas (CG) and treatment group (TG, Sunitinib treatment starting on day 10). Upper part: CX3CR1-eGFP positive cells - green, CD31 positive cells - red, cell nuclei - blue (DAPI), KI-67-positive cells - magenta: (A) CG. left, high microglia accumulation with association to tumor vessels. right, higher magnification image corresponding to inset on the left - high microglia accumulation with frequent contact to the vasculature. (B) TG. left, decreased microglia accumulation compared to CG, microglia clusters around therapy resistant tumor vessels encircled in white. Right, higher magnification corresponding to inset on the left - increased accumulation at vessel wall and around vessels compared to CG. (C) KI67 staining. left, merge - microglia, nuclei, vessels, KI-67-positive cells; white arrow - proliferating microglia; right, corresponding image with KI67 staining. (D) KI67 staining of BG. Left, merge - unique distribution of resting microglia cells with no proliferating cells. Right: corresponding image with KI67-staining. (E) overview of glioma on day 21 with microglia accumulation around and in tumor area. (F) high magnification of tumor vessel with large microglia-endothelial contact. (G) tumor border with high tumor vascularization (left) compared to surrounding brain parenchyma (right). Lower part: quantification of immunofluorescence. (H) vessel area is increased in gliomas, antiavascular therapy diminishes vessel area. (I) vessel density is tighter in CG compared to the TG. (J) microglia density is highly enhanced in CG; there is a decreased microglia accumulation in TG. (K) fraction of microglia co-localized to the vessel wall is increased in CG and even higher in TG. (L) significant fraction of KI-67-positive microglia was found in both tumor groups. (M) fraction of perivascular KI-67-positiv cells is lower compared to interstitial microglia.

microglia cells in physiological tissue. (Fig. 3F,G). In contrast, NOX activity measurements of the mobile phenotype could not be assessed. Because of the high cell motility in this phenotype we could not guarantee that FLIM measurements correspond to the microglia (CX3CR1-eGFP mask) mask recorded shortly before FLIM.

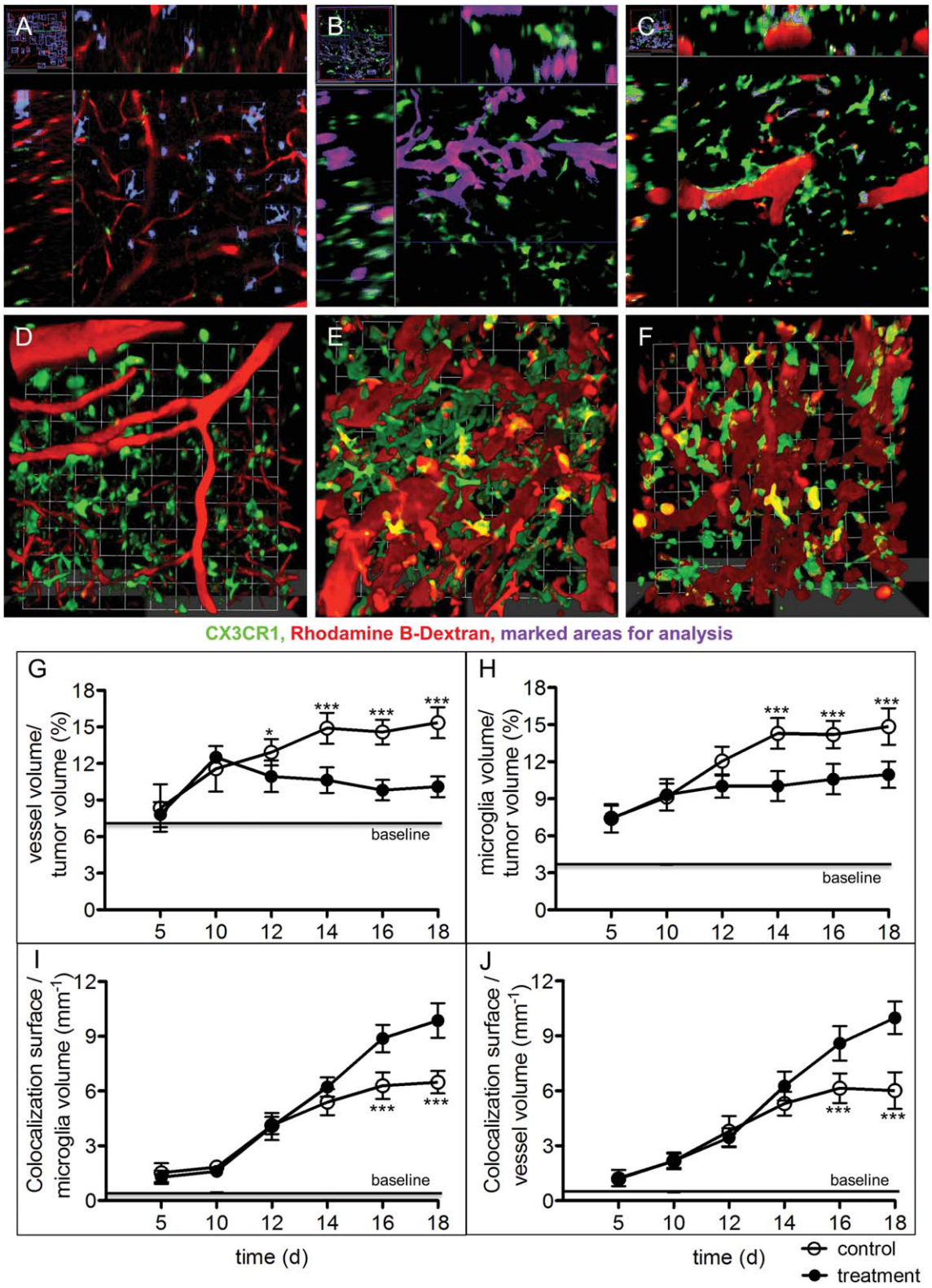

FIGURE 7.

Role of the Tumor Vessel Compartment for Microglia Behavior

Intravital time laps of microglia cells showed a high association of microglia cells to the tumor vasculature. Static microglia cells and especially the mobile phenotype colonized and migrated in the perivascular niche (Supporting Information Movie 6). Therefore, we assumed that the tumor vessel compartment is relevant for microglia migration *in vivo*. To evaluate this interdependency, we modulated the tumor vessel compartment using a pharmacological antivascular approach with Sunitinib starting on day 10 after tumor cell implantation and studied its effects on microglia behavior *in vivo*.

Tumor size and edema were measured by MRI volumetry. In the Sunitinib group, tumors were significantly smaller compared to the control group (Fig. 4A–C). In addition, we were able to observe a decrease in the edema size (Fig. 4A,B,D). The functionality of brain tumor blood vessels was investigated *in vivo* by epi-illuminating fluorescence video microscopy (IEFVM). In controls, the total vascular density (TVD) increased in the control group during the first 12 days of tumor growth, reflecting the high angiogenic activity of the model. (Fig. 5G). In the Sunitinib group, TVD was significantly reduced, resulting in an altered tumor vascular compartment (Fig. 5A–C). Tumor vessels in the control group showed an increased vascular leakage with a high permeability index. In contrast to that, the leakage was clearly reduced in animals, that received antivascular treatment (Fig. 5D–F). Taken together, microvessel density in anti-vascularly treated tumors is reduced but tumors have a distinct amount of therapy resistant vessels, which show a typical pattern of normalization (Czabanka et al., 2009) with a definite decrease of vessel leakage and reduced permeability in IEFVM and reduced edema in MRI imaging. Importantly, we performed additional *in vivo* staining of circulating white blood cells by Rhodamine 6G and studied their recruitment frequency to the tumor blood vessel wall. This allowed us to assess whether changes in the tumor vascular compartment would lead to an increased recruitment of granulocytes or myeloid cells from the periphery. If so, this would interfere with the interpretation of the behavior of our time-lapse microscopy. However, our analyses excluded a change in white blood cell/endothelial interactions and recruitment frequency (from initially physiological values) and, thus, confirmed that after the antivascular intervention CX3CR1-eGFP-positive cells still reflect resident microglia. (Fig. 5G) This confirmed the results, that have been published before, concerning immune cells in GL261 gliomas. (Müller et al., 2014)

In order to assess the effect of this significant change of the vascular compartment on microglia behavior and trafficking we first performed immunofluorescence staining after 21 days of tumor growth. Staining of tumor blood vessels with CD31 confirmed a significant antivascular change of initially highly vascularized tumors (Fig. 6G) by Sunitinib. Compared to control animals, vessel area and vessel density were significantly reduced (Fig. 6A,B,H,I). Iba-1 positive microglia cells accumulated preferably in the tumor (Fig. 6E). Interestingly, total microglia accumulation in the tumor area was diminished in the Sunitinib group (Fig. 6B,J). However, of the remaining microglia a higher percentage homed to the perivascular niche when compared to the control group (Fig. 6B,F,K). To rule out that these differences are due to a change in the proliferative activity of microglial cells we performed KI-67 labeling. In both groups, the overall KI-67 labeling index was around 10% (Fig. 6C,D,L), [2% for perivascular microglia (Fig. 6M)] suggesting that antivascular therapy indirectly changed the migratory behavior of microglial cells.

After sham implantation followed by the same Sunitinib protocol we could not observe a change in vessel density and formation as well as in microglia density and perivascular microglia accumulation in the physiological brain until the end of experiment (day 21) (Supporting Information Fig. 1).

To study whether the therapy-induced reduction of tumor-associated microglia goes along with a change of microglia migration pattern and to analyze changes of microglia trafficking kinetics, we applied intravital TPLSM again.

FIGURE 7: Microglia accumulation, vascular network and microglia-vessel co-localization surface measured by intravital Two-photon laser scanning microscopy in baseline group (physiological group without tumor). control group with GL261-glioma and treatment group (Sunitinib treatment starting on day 10). Upper part: representative 3D images of z-stack analysis and regions of interest in the three groups: (A) measurement of microglia volume (magenta) around vascular network (red) (B) measurement of vessel volume (magenta) with microglia (green) in between. (C) measurement of microglia-vessel co-localization surface (white) with microglia (green) and vessels (red). (D), physiological brain parenchyma with dendritic vascular network (red) and uniform distribution of not activated microglia cells (green). (E) control group with dense intratumoral microglia formation (green), tight-meshed vascular network (red) and with microglia association to the vessel walls (yellow). (F) treatment group with reduced vessel density and reduced microglia accumulation (green) but increased microglia-vessel contact (yellow). Lower part: Quantification of microglia accumulation, angiogenesis and co-localization in the three groups: (G) vessel volume increases during glioma progression, treatment reduces vascular density (H) increase of microglia volume during glioma growth, treatment group shows significant reduced microglia accumulation. (I) microglia-vessel co-localization surface/microglia volume increases during tumor development and is even higher in advanced stages of treated gliomas compared to control group. (J) microglia-vessel co-localization surface/ vessel volume increases during tumor development and is even higher in advanced stages of treated gliomas compared to control group. *$P < 0.05$, ***$P < 0.001$.

After a pretherapeutic increase of microglia cells during tumor development (Fig. 7D,E,I,J), we observed with the beginning of antivascular therapy a significant reduction of microglia cells parallel to the decrease of tumor blood vessels (Fig. 7E,F,G,H) and we found changes of the microglia trafficking kinetics. The microglia cells homing mainly in the perivascular area showed a higher activity compared to the control group. We discovered an absolute increase of the mobile microglia subtype fraction, very actively trafficking in the perivascular area.

Again the Sunitinib treatment in mice, which did not receive a tumor cell implantation, did not affect microglia kinetics or morphology.

Discussion

Our study gives an *in vivo* insight into microglia behavior and trafficking kinetics in malignant gliomas. Employing TPLSM in an orthotopic model we are able to perform repetitive real time imaging of microglia cells in different stages of the disease. We further demonstrated and verified the power of our model for screening new therapeutic approaches. Furthermore we could display the relevance of the tumor vasculature for microglia migration and accumulation in gliomas. The accumulation of tumor associated microglia cells can be reduced by a depletion of tumor vessels. Nevertheless diminished microglia in tumors, which received antivascular therapy, show a high activity and trafficking motility predominantly in the perivascular area.

Glioma-associated microglia acts differently compared to microglia cells in other disease models like neurodegenerative or trauma disease. They show an impressive change of their phenotype and behavior to a variety of heterogeneous cell subtypes, some of them with a highly increased motility and intratumoral trafficking. In contrast to earlier studies we observed a spectrum of three new tumor microglia subtypes. We classified them as (1) phagocytic, (2) interacting, and (3) mobile tumor-associated microglia cells. All cell subtypes present themself with unique cell shapes as well as cell sizes. Moreover microglia phenotypes have very variable movement patterns.

Whether the observed microglia subtypes illustrate different cell populations rather than different cell stages of intratumoral microglia cells, has to be confirmed in further studies. Nevertheless there is an enormous difference in cell size of these subtypes with one type being smaller than resident microglia and one type three times as big. Further the enzyme activity is markedly different. This indicates that these cell types might at least have different cell functions in the tumor milieu and influence tumor development differently.

Microglia subtypes participate differently in intratumoral oxidative stress. Cells with high motility show a low NADPH oxidase activity level, which is not increased compared to resting microglia cells. Presumably they are not involved in phagocytosis or responsible for cytotoxic effects in glioma microenvironment. They do not contribute relevantly to the ROS production. Whereas the phagocytic hypertrophic microglia subtype has a very high level of activated NOX, which implies cytotoxic and phagocytic functions (Chang et al., 2010). Under this precondition a tumor suppressing function of this cell type is most likely.

There are several studies that show an infiltration of monocyte-derived macrophages in experimental gliomas (Feng et al., 2015; Zhou et al., 2015). The possibility to differentiate between microglia and macrophages or monocytes by expression of CX3CR1 is highly controverse. Some studies distinguished between microglia and macrophages via the CX3CR1- and CCR2-expression. CX3CR1 is suggested to be microglia specific and macrophages should be CX3CR1-negativ or –low (Mizutani et al., 2012; Zhou et al., 2015). However there are several studies that illustrated blood monocytes to be CX3CR1-positive dependent on their activation level (Geissmann et al., 2003; Yona et al., 2013). Therefore we cannot clearly distinguish between microglia cells and monocyte-derived macrophages via CX3CR1- or IBA-1 expression in our model (Hambardzumyan et al., 2015). However in a recent study we could show that in the GL261-tumor model up to day 14 the monocyte/macrophage population is very low (2%) and we can assume that our CX3CR1-population on day 14 (used for intravital cell analysis) is nearly a pure microglia population and the indicated phenotypes belong to microglia cells (Müller et al., 2014).

The influence of CX3CR1 receptors on glioma development and on microglia is discussed controversely. An influence of CX3CR1 expression on optic glioma formation in mice with Neurofibromatosis-1 was shown (Pong et al., 2013). However, Liu et al. and Feng et al. illustrated that a complete loss of CX3CR1 does neither affect the microglia infiltration nor their formation in experimental gliomas (Feng et al., 2015; Liu et al., 2008). Feng et al. showed merely an increased monocyte infiltration in tumors and a more aggressive growth of these tumors in animals with a complete loss of CX3CR1. In our experimental glioma model microglial CX3CR1 is only reduced and as we could show in our previous publication on day 14 the monocyte infiltration is marginal and myeloid cells in the tumor demonstrate about a nearly pure microglia population. Therefore the influence of monocyte infiltration should not affect the tumor development in our tumor model up to day 14 significantly (Müller et al., 2014). All the movies, which were used for microglia phenotyping (represented in Supporting Information movies),

show microglia cells up to day 14. Comparing the tumor growth and microglia formation of GL261 tumors in wild type C57BL/6 and CX3CR1$^{GFP/wt}$ animals we could neither detect a difference in microglia density and perivascular microglia density nor in vessel density or vessel area (Supporting Information Fig. 2). Therefore, we do not think that the heterogeneous binding of GFP on the CX3CR1 effects the microglia infiltration or behavior in our model.

Microglia cell accumulation in gliomas takes place in parallel to tumor angiogenesis. Microglia migration and influx into the tumor tissue can be reduced by antivascular therapy, without affecting microglia proliferation. A high association of activated microglia cells to the perivascular niche supports the importance of angiogenesis for microglia migration into the tumor mass. Especially the mobile microglia phenotype moves directly at the vessel walls with a very high cell velocity compared to typical microglia movement patterns. Microglia with contact to the vessel walls have a low fraction of proliferating cells. The perivascular niche is predominantly used for migration and interaction whereas the proliferation takes place in the interstitial space. Microglia-tumor vessel interaction was increasingly observable during tumor progression. Therefore tumor angiogenesis might substantially influence microglia migration or proliferation in malignant gliomas.

Growth of high-grade gliomas is dependent on a rapid tumor angiogenesis. A high level of vascularization is essential for tumor development in order to reach a significant tumor mass. Therefore many therapeutic approaches have set their target on the inhibition of angiogenesis in order to stop glioma progression (Ferrara and Kerbel, 2005; Norden et al., 2008). One of the most important and well-known growths factors that influences glioma angiogenesis, is the vascular endothelial growth factor (VEGF) (Ferrara, 2002). Bevacizumab, a monoclonal antibody directed against the subtype VEGF-A, as well as tyrosine kinase inhibitors such as Sorafenib and Sunitinib that target the VEGF-receptor (VEGFR) and the platelet-derived growths factor receptor (PDGFR), are antiangiogenic compounds established for the treatment of various peripheral tumor types. Recently, Bevacizumab was shown to significantly prolong progression free survival in patients with newly diagnosed glioblastoma (Chinot et al., 2014).

Our study highlights the influence of antivascular therapy on microglia migration. As expected, we could demonstrate that gliomas, treated with antivascular therapy, are substantially smaller than not treated tumors. A significantly reduced vascular scaffold leads in parallel to a significant reduction of microglia cells in gliomas. The residual microglia cells show a higher association to tumor vessels. The microglia migration is most lively in the perivascular space as illustrated in TPLSCM and histological analysis. In total we found a decrease of microglia cells but an absolute increase of the number of the mobile microglia subtype. This mobile subtype characteristically shows a preference for the perivascular space where they interact with the abluminal endothelial cell surface and peri-endothelial support cells (i.e., pericytes).

Our results lead to the hypothesis that the vascular network of gliomas is a scaffold with guidance cues for microglia infiltration into the tumor area. The perivascular area plays an important role, which serves as a highway for microglia trafficking. In antivascular treated tumors the therapy resistant tumor vessels are even more used by microglia cells with a high migration activity. This gives evidence for the importance of the vascular network for microglia migration.

The resident microglia of the brain plays a key role in the development of malignant gliomas. The precise function of microglia cells in the tumor micromilieu is only fragmentary understood. To expand the knowledge of tumor microglia function and to generate novel therapy options, a detailed analysis and differentiated classification of the cell phenotypes and their behavior is pending. Several studies described tumor associated microglia cells only as generally activated microglia cells with a hypertrophic cell body and reduced ramified processes. These studies were only performed in different *ex vivo* or *in vitro* glioma models or in other CNS-disease models. However, we know about the oppositional functions of microglia cells in primary brain tumors. In consequence there must be more versatile phenotypes. This is one of the first studies, which shows an intravital recording of microglia behavior in malignant gliomas and clearly demonstrates the actual appearance, motility and variety of tumor-associated microglia phenotypes. Our intravital study enables a deep insight into microglia practice in glioma tissue. Instead of only a resting phenotype in physiological brain parenchyma and an activated phenotype in and around the glioma we discovered three, novel, completely different microglia subtypes in deep tissue Two-photon imaging of malignant gliomas. To develop an understanding what kind of tumor therapy is influencing microglia in what way, all different phenotypes should be considered separately. Therefore different microglia subtypes with contrary functions should be investigated. The relevance for tumor development and therapy options needs further investigations.

Acknowledgment

Grant sponsor: Deutsche Forschungsgemeinschaft; Grant number: SFB TRR 43 (to P.V.) and NI1167/3-1 (JIMI) (to R.N. and Z.C.)

The authors thank all members of the Joint intravital microscopy and Imaging Network (JIMI) for hardware support and intellectual exchange. In addition, the authors thank

Thomas Broggini for mouse breeding management and establishing of genotyping protocols.

References

Baatz H, Steinbauer M, Harris AG, Krombach F. 1995. Kinetics of white blood cell staining by intravascular administration of rhodamine 6G. Int J Microcirc Clin Exp [Internet] 15:85–91.

Chang W, Yang Y, Lu H, Li I, Liau I. 2010. Spatiotemporal characterization of phagocytic NADPH oxidase and oxidative destruction of intraphagosomal organisms in vivo using autofluorescence imaging and Raman microspectroscopy. J Am Chem Soc [Internet] 132:1744–1745.

Chinot OL, Wick W, Mason W, Henriksson R, Saran F, Nishikawa R, Carpentier AF, Hoang-Xuan K, Kavan P, Cernea D, Brandes A. a, Hilton M, Abrey L, Cloughesy T. 2014. Bevacizumab plus radiotherapy-temozolomide for newly diagnosed glioblastoma. N Engl J Med [Internet] 370:709–722.

Coniglio SJ, Eugenin E, Dobrenis K, Stanley ER, West BL, Symons MH, Segall JE. 2012. Microglial stimulation of glioblastoma invasion involves epidermal growth factor receptor (EGFR) and colony stimulating factor 1 receptor (CSF-1R) signaling. Mol Med [Internet] 18:519–527.

Czabanka M, Vinci M, Heppner F, Ullrich A, Vajkoczy P. 2009. Effects of sunitinib on tumor hemodynamics and delivery of chemotherapy. 1300:1293–1300.

Davalos D, Grutzendler J, Yang G, Kim JV, Zuo Y, Jung S, Littman DR, Dustin ML, Gan W-B. 2005. ATP mediates rapid microglial response to local brain injury in vivo. Nat Neurosci [Internet] 8:752–758.

Feng X, Szulzewsky F, Yerevanian A, Chen Z, Heinzmann D, Rasmussen RD, Alvarez-Garcia V, Kim Y, Wang B, Tamagno I, Zhou H, Li X, Kettenmann H, Ransohoff RM, Hambardzumyan D. 2015. Loss of CX3CR1 increases accumulation of inflammatory monocytes and promotes gliomagenesis. Oncotarget [Internet] 6:15077–15094.

Ferrara N, Kerbel RS. 2005. Angiogenesis as a therapeutic target. Nature [Internet] 438:967–974.

Ferrara N. 2002. VEGF and the quest for tumour angiogenesis factors. Nat Rev Cancer [Internet] 2:795–803.

Flügel A, Labeur MS, Grasbon-Frodl EM, Kreutzberg GW, Graeber MB. 1999. Microglia only weakly present glioma antigen to cytotoxic T cells. Int J Dev Neurosci [Internet] 17:547–556.

Galarneau H, Villeneuve J, Gowing G, Julien J, Vallières L. 2007. Increased glioma growth in mice depleted of macrophages. Cancer Res [Internet] 67: 8874–8881.

Geissmann F, Jung S, Littman DR. 2003. Blood monocytes consist of two principal subsets with distinct migratory properties. Immunity [Internet] 19: 71–82.

Graeber MB, Scheithauer BW, Kreutzberg GW. 2002. Microglia in brain tumors. Glia [Internet] 40:252–259.

Hambardzumyan D, Gutmann DH, Kettenmann H. 2015. The role of microglia and macrophages in glioma maintenance and progression. Nat Neurosci [Internet] 19:20–27.

Hefendehl JK, Neher JJ, Sühs RB, Kohsaka S, Skodras A, Jucker M. 2014. Homeostatic and injury-induced microglia behavior in the aging brain. Aging Cell [Internet] 13:60–69.

Hines DJ, Hines RM, Mulligan SJ, Macvicar B. a. 2009. Microglia processes block the spread of damage in the brain and require functional chloride channels. Glia [Internet] 57:1610–1618.

Hussain SF, Kong L-Y, Jordan J, Conrad C, Madden T, Fokt I, Priebe W, Heimberger AB. 2007. A novel small molecule inhibitor of signal transducers and activators of transcription 3 reverses immune tolerance in malignant glioma patients. Cancer Res [Internet] 67:9630–9636.

Kielian T, van Rooijen N, Hickey WF. 2002. MCP-1 expression in CNS-1 astrocytoma cells: Implications for macrophage infiltration into tumors in vivo. J Neurooncol [Internet] 56:1–12.

Kloss CU, Bohatschek M, Kreutzberg GW, Raivich G. 2001. Effect of lipopolysaccharide on the morphology and integrin immunoreactivity of ramified microglia in the mouse brain and in cell culture. Exp Neurol [Internet] 168: 32–46.

Kozlowski C, Weimer RM. 2012. An automated method to quantify microglia morphology and application to monitor activation state longitudinally in vivo. PLoS One [Internet] 7:e31814.

Lakowicz JR, Szmacinski H, Nowaczyk K, Johnson ML. 1992. Fluorescence lifetime imaging of free and protein-bound NADH. Proc Natl Acad Sci U S A [Internet] 89:1271–1275.

Liu C, Luo D, Streit WJ, Harrison JK. 2008. CX3CL1 and CX3CR1 in the GL261 murine model of glioma: CX3CR1 deficiency does not impact tumor growth or infiltration of microglia and lymphocytes. J Neuroimmunol [Internet] 198:98–105.

Mabray MC, Barajas RF, Cha S. 2015. Modern Brain Tumor Imaging. Brain Tumor Res Treat [Internet] 3:8.

Markovic DS, Vinnakota K, Chirasani S, Synowitz M, Raguet H, Stock K, Sliwa M, Lehmann S, Kälin R, van Rooijen N, Holmbeck K, Heppner FL, Kiwit J, Matyash V, Lehnardt S, Kaminska B, Glass R, Kettenmann H. 2009. Gliomas induce and exploit microglial MT1-MMP expression for tumor expansion. Proc Natl Acad Sci U S A [Internet] 106:12530–12535.

Mizutani M, Pino PA, Saederup N, Charo IF, Ransohoff RM, Cardona AE. 2012. The fractalkine receptor but not CCR2 is present on microglia from embryonic development throughout adulthood. J Immunol [Internet] 188: 29–36.

Morimura T, Neuchrist C, Kitz K, Budka H, Scheiner O, Kraft D, Lassmann H. 1990. Monocyte subpopulations in human gliomas: Expression of Fc and complement receptors and correlation with tumor proliferation. Acta Neuropathol [Internet] 80:287–294.

Morioka T, Baba T, Black KL, Streit WJ. 1992. Response of microglial cells to experimental rat glioma. Glia [Internet] 6:75–79.

Müller A, Brandenburg S, Turkowski K, Müller S, Vajkoczy P. 2014. Resident microglia, and not peripheral macrophages, are the main source of brain tumor mononuclear cells. Int J Cancer [Internet] 1–11.

Niesner R, Narang P, Spiecker H, Andresen V, Gericke K-H, Gunzer M. 2008. Selective detection of NADPH oxidase in polymorphonuclear cells by means of NAD(P)H-based fluorescence lifetime imaging. J Biophys [Internet] 2008: 602639.

Nimmerjahn A, Kirchhoff F, Helmchen F. 2005. Resting microglial cells are highly dynamic surveillants of brain parenchyma in vivo. Science [Internet] 308:1314–1318.

Norden AD, Drappatz J, Wen PY. 2008. Novel anti-angiogenic therapies for malignant gliomas. Lancet Neurol [Internet] 7:1152–1160.

Oh T, Fakurnejad S, Sayegh ET, Clark AJ, Ivan ME, Sun MZ, Safaee M, Bloch O, James CD, Parsa AT. 2014. Immunocompetent murine models for the study of glioblastoma immunotherapy. J Transl Med [Internet] 12: 107.

Pong WW, Higer SB, Gianino SM, Emnett RJ, Gutmann DH. 2013. Reduced microglial CX3CR1 expression delays neurofibromatosis-1 glioma formation. Ann Neurol [Internet] 73:303–308.

Pope WB, Sayre J, Perlina A, Villablanca JP, Mischel PS, Cloughesy TF. 2005. MR imaging correlates of survival in patients with high-grade gliomas. AJNR Am J Neuroradiol [Internet] 26:2466–74.

Pyonteck SM, Akkari L, Schuhmacher AJ, Bowman RL, Sevenich L, Quail DF, Olson OC, Quick ML, Huse JT, Teijeiro V, Setty M, Leslie CS, Oei Y, Pedraza A, Zhang J, Brennan CW, Sutton JC, Holland EC, Daniel D, Joyce JA. 2013. CSF-1R inhibition alters macrophage polarization and blocks glioma progression. Nat Med [Internet] 19:1264–1272.

Roggendorf W, Strupp S, Paulus W. 1996. Distribution and characterization of microglia/macrophages in human brain tumors. Acta Neuropathol [Internet] 92:288–293.

Sahm F, Oezen I, Opitz C. a, Radlwimmer B, von Deimling A, Ahrendt T, Adams S, Bode HB, Guillemin GJ, Wick W, Platten M. 2013. The endogenous

tryptophan metabolite and NAD+ precursor quinolinic acid confers resistance of gliomas to oxidative stress. Cancer Res [Internet] 73:3225–3234.

Sarkar S, Döring A, Zemp FJ, Silva C, Lun X, Wang X, Kelly J, Hader W, Hamilton M, Mercier P, Dunn JF, Kinniburgh D, van Rooijen N, Robbins S, Forsyth P, Cairncross G, Weiss S, Yong VW. 2013. Therapeutic activation of macrophages and microglia to suppress brain tumor-initiating cells. Ann Neurosci [Internet] 20:154.

Shinonaga M, Chang CC, Suzuki N, Sato M, Kuwabara T. 1988. Immunohistological evaluation of macrophage infiltrates in brain tumors. Correlation with peritumoral edema. J Neurosurg [Internet] 68:259–265.

Tremblay M-È, Lowery RL, Majewska AK. 2010. Microglial interactions with synapses are modulated by visual experience. PLoS Biol [Internet] 8: e1000527.

Vajkoczy P, Schilling L, Ullrich A, Schmiedek P, Menger MD. 1998. Characterization of angiogenesis and microcirculation of high-grade glioma: An intravital multifluorescence microscopic approach in the athymic nude mouse. J Cereb Blood Flow Metab [Internet] 18:510–520.

Wake H, Moorhouse AJ, Jinno S, Kohsaka S, Nabekura J. 2009. Resting microglia directly monitor the functional state of synapses in vivo and determine the fate of ischemic terminals. J Neurosci [Internet] 29:3974–3980.

Wang S-C, Hong J-H, Hsueh C, Chiang C-S. 2012. Tumor-secreted SDF-1 promotes glioma invasiveness and TAM tropism toward hypoxia in a murine astrocytoma model. Lab Invest [Internet] 92:151–162.

Wei J, Gabrusiewicz K, Heimberger A. 2013. The controversial role of microglia in malignant gliomas. Clin Dev Immunol [Internet] 2013:285246.

Winkler F, Kienast Y, Fuhrmann M, Von Baumgarten L, Burgold S, Mitteregger G, Kretzschmar H, Herms J. 2009. Imaging glioma cell invasion in vivo reveals mechanisms of dissemination and peritumoral angiogenesis. Glia [Internet] 57:1306–1315.

Yona S, Kim K-W, Wolf Y, Mildner A, Varol D, Breker M, Strauss-Ayali D, Viukov S, Guilliams M, Misharin A, Hume DA, Perlman H, Malissen B, Zelzer E, Jung S. 2013. Fate mapping reveals origins and dynamics of monocytes and tissue macrophages under homeostasis. Immunity [Internet] 38:79–91.

Yuan F, Salehi HA, Boucher Y, Vasthare US, Tuma RF, Jain RK. 1994. Vascular permeability and microcirculation of gliomas and mammary carcinomas transplanted in rat and mouse cranial windows. Cancer Res [Internet] 54:4564–4568.

Zemp FJ, McKenzie B. a, Lun X, Reilly KM, McFadden G, Yong VW, Forsyth PA. 2014. Cellular factors promoting resistance to effective treatment of glioma with oncolytic myxoma virus. Cancer Res [Internet] 74:7260–7273.

Zhai H, Heppner FL, Tsirka SE. 2011. Microglia/macrophages promote glioma progression. Glia [Internet] 59:472–485.

Zhou W, Ke SQ, Huang Z, Flavahan W, Fang X, Paul J, Wu L, Sloan AE, McLendon RE, Li X, Rich JN, Bao S. 2015. Periostin secreted by glioblastoma stem cells recruits M2 tumour-associated macrophages and promotes malignant growth. Nat Cell Biol [Internet] 17:170–182.

Legends for supplementary figures and supplementary movies:

Supplementary figure 1:

Comparison of CX3CR1$^{GFP/wt}$ mice with and without Sunitinib treatment under physiological conditions 21 days after cell implantation

(A + B) representative immunofluorescence with microglia (CX3CR1-positive cells, green), vessels (CD 31-positive cells, red) and nuclei (DAPI, blue) in the normal brain without Sunitinib treatment **(A)** and after 10 days of Sunitinib treatment **(B)**. Quantification shows no difference in antivascular treated animals without GL261-cell implantation compared to not treated animals concerning microglia density **(C)**, perivascular microglia accumulation **(D)**, vessel area **(E)** and vessel density **(F)**.

Supplementary figure 2:

Comparison of GL261 gliomas in CX3CR1$^{GFP/wt}$ mice and wildtype C57BL/6 mice 21 days after cell implantation

(A + B) representative immunofluorescence with microglia (IBA-1 positive cells, magenta/CX3CR1-positive cells, green), vessels (CD 31-positive cells, red) and nuclei (DAPI, blue) in GL261 gliomas in wildtype C57BL/6 mice **(A)** and CX3CR1$^{GFP/wt}$ mice **(B)**. There is no difference in gliomas of wildtype mice compared to CX3CR1$^{GFP/wt}$ mice concerning microglia density **(C)**, perivascular microglia accumulation **(D)**, vessel area **(E)**, and vessel density **(F)**

Movie 1:

30 minutes- time lapse with intravital 2-photon laser scanning microscopy in baseline group, CX3CR1-eGFP-positive microglia in green, rhodamine B-dextran enhanced vessels in red.

Not activated microglia under physiological conditions. Only a movement of the cellular processes can be observed.

Movie 2:

60 minutes- time lapse with intravital 2-photon laser scanning microscopy in tumor group, CX3CR1-eGFP-positive microglia in green, rhodamine B-dextran enhanced vessels in red. (day 14 after tumor cell implantation)
Tumor associated microglia shows a high heterogeneity of microglia cell movements and sizes.

Movie 3:

60 minutes- time lapse with intravital 2-photon laser scanning microscopy in tumor group, CX3CR1-eGFP-positive microglia in green, intracellular autofluorescence in orange (day 14 after tumor cell implantation);
Hypertrophic, bearly moving tumor associated microglia cell with autofluorescence spots, suggestive for phagocytosis – phagocytic subtype.

Movie 4:

60 minutes- time lapse with intravital 2-photon laser scanning microscopy in tumor group, CX3CR1-eGFP-positive microglia in green (day 14 after tumor cell implantation);
Microglia cell with actively probing processes an dynamic cell shape changes - interacting subtype.

Movie 5:

60 minutes- time lapse with intravital 2-photon laser scanning microscopy in tumor group, CX3CR1-eGFP-positive microglia in green, rhodamine B-dextran enhanced vessels in red. (day 14 after tumor cell implantation);
Microglia cell with amoeboid like cell shape changes and fast movement through the tumor area – mobile subtype.

Movie 6:

60 minutes- time lapse with intravital 2-photon laser scanning microscopy in tumor group, CX3CR1-eGFP-positive microglia in green, rhodamine B-dextran enhanced vessels in red. (day 14 after tumor cell implantation);
Microglia in the perivascular area show a very high motility and the mobile phenotype is accumulating in this area.

Supplementary Figure 1

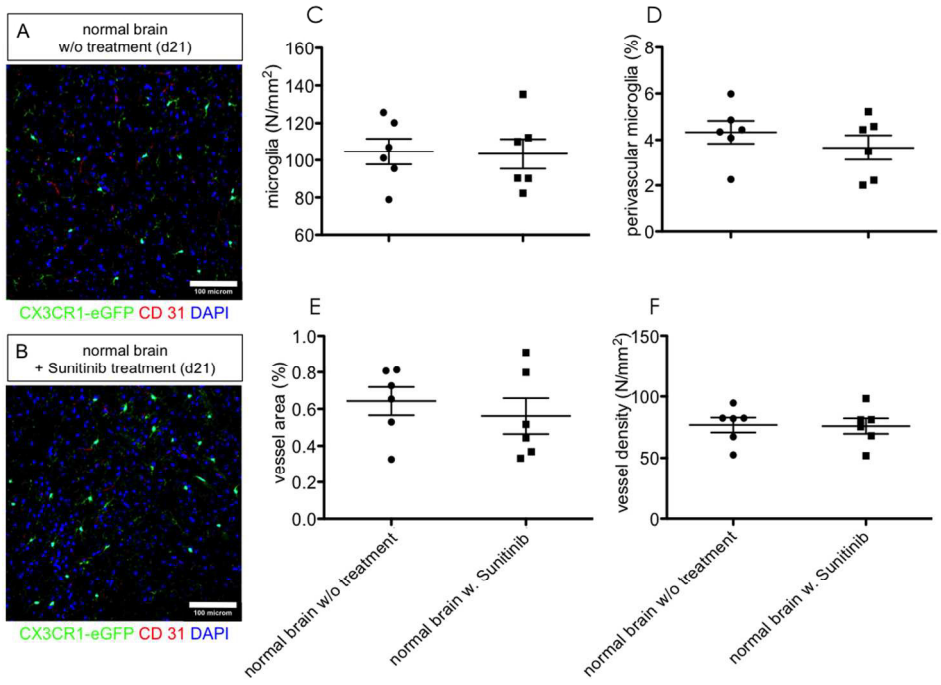

423x317mm (72 x 72 DPI)

Supplementary Figure 2

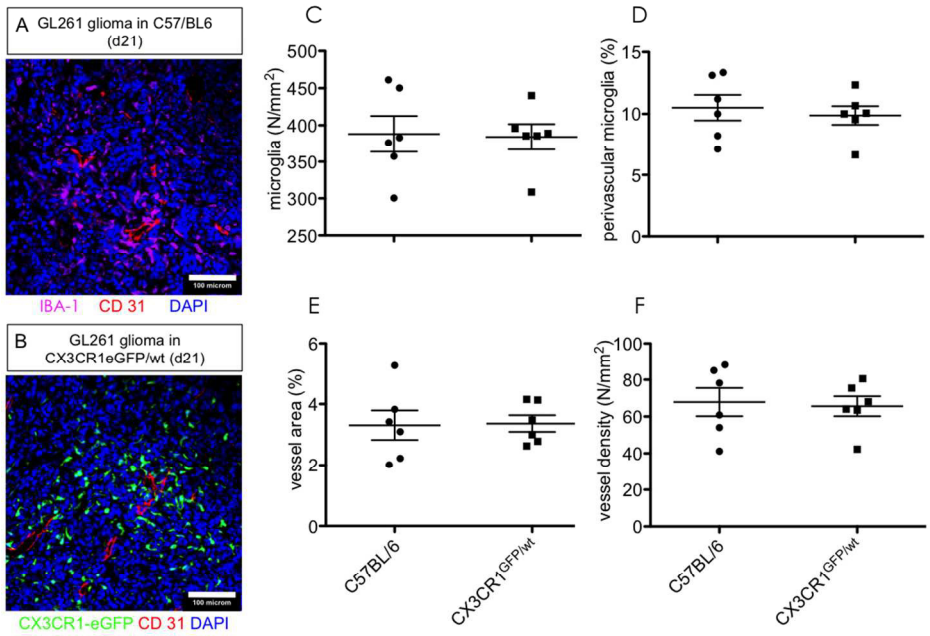

423x317mm (72 x 72 DPI)

Mein Lebenslauf wird aus datenschutzrechtlichen Gründen in der elektronischen Version meiner Arbeit nicht veröffentlicht.

Mein Lebenslauf wird aus datenschutzrechtlichen Gründen in der elektronischen Version meiner Arbeit nicht veröffentlicht.

7. Publikationsliste

Publikationen in peer-reviewed journals:

1. **Bayerl SH** and Pöhlmann F, Finger T, Franke J, Woitzik J, Vajkoczy P (2016) The Sagittal Spinal Profile Type - a principal precondition for surgical decision-making in patients with lumbar spinal stenosis. *J Neurosurg Spine* in revision
   impact factor 2,126

2. **Bayerl SH**, Melina Nieminen, Thomas Broggini, Peter Vajkoczy, Vincent Prinz (2016) Craniotomy plus distal stroke surgery for chronic brain imaging in ischemia. *J Vis Exp.*, accepted
   impact 1,325

3. Onken J, Reinke A, Radke J, Finger T, **Bayerl S**, Vajkoczy P, Meyer B (2016) Revision surgery for cervical artificial disc: Surgical technique and clinical results. *Clin Neurol Neurosurg* 2016 152:39-44.
   impact factor: 1,198

4. Finger T, **Bayerl S**, Bertog M, Czabanka M, Woitzik J, Vajkoczy P. Impact of sacropelvic fixation on the development of postoperative sacroiliac joint pain following multilevel stabilization for degenerative spine disease. *Clin Neurol Neurosurg* 150:18-22
   impact factor: 1,198

5. **Bayerl SH**, Niesner R, Cseresnyes Z, Radbruch R, Pohlan J, Brandenburg S, Czabanka MA, Vajkoczy P (2016) Time Lapse *In Vivo* Microscopy Reveals distinct dynamics of microglia-tumor environment interactions – a new role for the tumor perivascular space as highway for trafficking microglia. *Glia* 64(7):1210-26
   Impact factor 6,031

6. Prinz V, Finger T, **Bayerl S**, Rosenthal C, Wolf S, Liman T, Vajkoczy P (2016) High prevalence of pharmacologically induced platelet dysfunction in the acute setting of brain injury. *Acta Neurochir (Wien)* 158:117–123

impact factor 1,766

7. **Bayerl SH**, Pöhlmann F, Finger T, Onken J, Franke J, Czabanka M, Woitzik J, Vajkoczy P (2015) The sagittal balance does not influence the one year clinical outcome of patients with lumbar spinal stenosis without obvious instability after microsurgical decompression. *Spine (Phila Pa 1976)* 40:1
impact factor 2,297

8. Streitberger K-J, Reiss-Zimmermann M, Freimann FB, **Bayerl S**, Guo J, Arlt F, Wuerfel J, Braun J, Hoffmann K-T, Sack I (2014) High-Resolution Mechanical Imaging of Glioblastoma by Multifrequency Magnetic Resonance Elastography Zhan W, ed. *PLoS One* 9:e110588
impact factor 3,234

9. Finger T, **Bayerl S**, Onken J, Czabanka M, Woitzik J, Vajkoczy P (2014) Sacropelvic fixation versus fusion to the sacrum for spondylodesis in multilevel degenerative spine disease. *Eur Spine J* 23:1013–1020
impact factor 2.066

10. **Bayerl S**, Wiendieck K, Koeppen D, Topalovic M, Übelacker A, Kroppenstedt S, Cabraja M (2013) Single- and multi-level anterior decompression and fusion for cervical spondylotic myelopathy--a long term follow-up with a minimum of 5 years. *Clin Neurol Neurosurg* 115:1966–1971
impact factor 1,248

11. Czabanka M, Bruenner J, Parmaksiz G, Broggini T, Topalovic M, **Bayerl SH**, Auf G, Kremenetskaia I, Nieminen M, Jabouille a, Mueller S, Harms U, Harms C, Koch a, Heppner FL, Vajkoczy P (2013) Combined temozolomide and sunitinib treatment leads to better tumour control but increased vascular resistance in O6-methylguanine methyltransferase-methylated gliomas. *Eur J Cancer* 49:2243–2252
impact factor 4,819

12. Beier AD, Vachhrajani S, Bayerl SH, Aguilar CYD, Lamberti-Pasculli M, Drake JM (2012) Rotatory subluxation: experience from the Hospital for Sick Children. J Neurosurg Pediatr 9:144–148,
impact factor 1,628

13. Czabanka M, Parmaksiz G, **Bayerl SH**, Nieminen M, Trachsel E, Menssen HD, Erber R, Neri D, Vajkoczy P (2011) Microvascular biodistribution of L19-SIP in angiogenesis targeting strategies. *Eur J Cancer* 47:1276–1284,
impact factor 5,536

Kongressbeiträge:

1. Jahrestagung der Deutschen Gesellschaft für Wirbelsäulenchirurgie (Hannover 12/2016), **Bayerl SH**, Finger T, Heiden P, Dengler J, Vajkoczy P, Iliosakralgelenk-Syndrom - Ein Vergleich von zwei Elektroden für die Radiofrequenz-basierte Denervation

2. Jahrestagung der Deutschen Gesellschaft für Neurochirurgie (Frankfurt 06/2016), **Bayerl SH**, Finger T, Heiden P, Dengler J, Vajkoczy P, Iliosakralgelenk-Syndrom - Sacroiliac Joint Pain - a comparison oft two probes for radiofrequency treatmen

3. Jahrestagung der Deutschen Gesellschaft für Wirbelsäulenchirurgie (Frankfurt 12/2015), **Bayerl SH**, Pöhlmann F, Prinz V, Finger T, Vajkoczy P, 2-Höhen Korporektomie - ist eine zusätzliche dorsale Stabilisierung notwendig?

4. Jahrestagung der Deutschen Gesellschaft für Neurochirurgie (Karlsruhe 06/2015), **Bayerl SH**, Prinz V, Finger T, Pöhlmann F, Vajkoczy P, 2-level corpectomy - is an additional posterior fusion needed?

5. Jahrestagung der Deutschen Gesellschaft für Neurochirurgie (Karlsruhe 06/2015, Session – Beste Vorträge), **Bayerl SH**, Poehlmann F, Finger T, Onken J, Franke J, Czabanka MA, Woitzik J, Vajkoczy P, Sagittal balance und surgical therapy of lumbar spinal canal stenosis

6. Sektion Wirbelsäule der Deutschen Gesellschaft für Neurochirurgie (Innsbruck 09/2014, Session – Beste Vorträge), **Bayerl SH**, Poehlmann F, Finger T, Onken J, Franke J, Czabanka MA, Woitzik J, Vajkoczy P, Sagittal balance und surgical therapy of lumbar spinal canal stenosis

7. Tagung der Deutschen Gesellschaft für Interventionen an der Wirbelsäule (Berlin, 11/2015), **Bayerl SH**, Finger T, Heiden P, Prinz V, Dengler J, Vajkoczy P, Simplicity zur Therapie des ISG-Syndroms?

8. Young Investigator Meeting- Neuroonkologie (Gut Liebenberg, 02/2015), **Bayerl SH**, Niesner R, Cseresnyes Z, Radbruch H, Pohlan J, Brandenburg S, Czabanka MA, Vajkoczy P, In vivo visualization of migroglia-endothelial cell interaction in an experimental glioma model

9. Jahrestagung der Deutschen Gesellschaft für Neurochirurgie (Dresden 05/2014), **Bayerl SH**, Poehlmann F, Finger T, Vajkoczy P, Sagittal profile influences the clinical outcome in patients with lumbar spinal stenosis after decompressive surgery

10. Jahrestagung der Deutschen Gesellschaft für Neurochirurgie (Düsseldorf 2013), **Bayerl SH**, Czabanka M, Brandenburg S, Cseresnyes Z, Niesner R, Vajkoczy P, Increased Microglia Motility with Association to Tumor Microvasculature in Malignant Gliomas

11. Jahrestagung der Deutschen Gesellschaft für Wirbelsäulenchirurgie (Frankfurt 12/2013), **Bayerl SH**, Pöhlmann F, Finger T, Vajkoczy P, The sagittal profile influences the clinical outcome in patients with lumbar spinal stenosis after decompressive surgery,
12. 7th International Symposium on the Biology of Endothelial Cells (Wien 2009), **Bayerl SH**, Czabanka M, Hakyi N, Vajkoczy P, In Vivo Characterization of a Murine Syngeneic Glioma Model in the Chronic Cranial Window

9. Danksagung

In erster Linie möchte ich mich bei meinem Doktorvater und Klinikdirektor Herrn Prof. Dr. Peter Vajkoczy bedanken für die Betreuung und die anregende wissenschaftliche Diskussion, welche essenziell für den Fortlauf dieser Arbeit gewesen sind. Durch ihn wurde mir mit einer ausgezeichneten Infrastruktur im Labor, durch Kontakte zu anderen Forschungsgruppen und natürlich auch insbesondere durch die finanziellen Mittel ermöglicht diese Arbeit durchzuführen, zu Ende zu bringen und einen tiefen Einblick in das experimentelle Arbeiten im Labor zu erhalten. Nicht zuletzt hat mich diese Arbeit dazu bewegt, nachdem ich Erfahrung mit tierexperimentellen mikrochirurgischen Operationen gesammelt habe und einen Einblick in die Vielfältigkeit und Faszination der Neurowissenschaften erhalten habe, auch die Facharztausbildung für Neurochirurgie in der Abteilung von Prof. Vajkoczy aufzunehmen.

Außerdem möchte ich mich ganz herzlich bei Herrn PD Dr. med. Marcus Czabanka bedanken. Von ihm wurde ich in das Arbeiten im Labor eingeführt und auch immer mit wertvollen Ratschlägen und Hinweisen unterstützt. Gleiches gilt auch für die klinische Ausbildung durch ihn.

Weiterhin möchte ich mich bei der JIMI-Arbeitsgruppe bedanken, insbesondere bei Frau Dr. Raluca Niesner und Herrn Dr. Zoltán Cseresnyés aus dem DRFZ, welche mir immer zur Seite standen, sich viel Zeit für mich und die Arbeit am Zwei-Photonen-Fluoreszenzmikroskop und die Auswertung der Ergebnisse genommen haben.

Ich danke außerdem Frau Melina Nieminen, Frau Irina Krementskaya, Frau Nahid Hakiy sowie Frau Dr. Susan Brandenburg für ihre forwährende Unterstützung in unserem Labor.

Ein besonderer Dank gilt meiner Familie und besonders meiner geliebten Ehefrau Dr. Nazli Esfahani-Bayerl für ihre Unterstützung, Motivation und Liebe, die mir ermöglicht haben meine Forschung parallel zu der zeitintensiven klinischen Arbeit durchzuführen.